cmgh
CELLULAR AND MOLECULAR GASTROENTEROLOGY AND HEPATOLOGY

ORIGINAL RESEARCH

Nedd4-2–dependent Ubiquitination Potentiates the Inhibition of Human NHE3 by Cholera Toxin and Enteropathogenic *Escherichia coli*

Kayte A. Jenkin,[1,2,*] Yiran Han,[1,3,*] Songbai Lin,[1,3,*] Peijian He,[1] and C. Chris Yun[1,3,4]

[1]Division of Digestive Diseases, Department of Medicine, Emory University School of Medicine, Atlanta, Georgia; [2]School of Science, Western Sydney University, Campbelltown, NSW 2560, Australia; [3]Atlanta VA Medical Center, Decatur, Georgia; and [4]Winship Cancer Institute, Emory University School of Medicine, Atlanta, Georgia

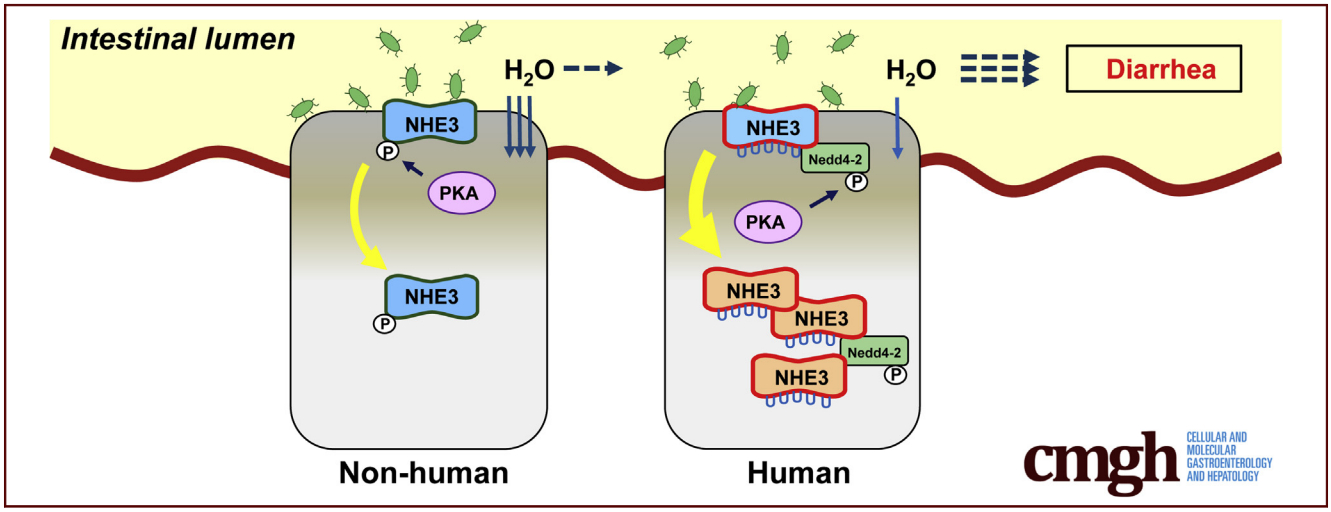

SUMMARY

Inhibition of Na^+/H^+ exchanger NHE3 in the intestine is a major cause of diarrhea. Using humanized mice expressing human NHE3, we explore the unique properties of hNHE3 that contribute to diarrheal symptoms occurring in humans.

BACKGROUND & AIMS: Diarrhea is one of the most common illnesses and is often caused by bacterial infection. Recently, we have shown that human Na^+/H^+ exchanger NHE3 (hNHE3), but not non-human NHE3s, interacts with the E3 ubiquitin ligase Nedd4-2. We hypothesize that this property of hNHE3 contributes to the increased severity of diarrhea in humans.

METHODS: We used humanized mice expressing hNHE3 in the intestine ($hNHE3^{int}$) to compare the contribution of hNHE3 and mouse NHE3 to diarrhea induced by cholera toxin (CTX) and enteropathogenic *Escherichia coli* (EPEC). We measured Na^+/H^+ exchange activity and fluid absorption. The role of Nedd4-2 on hNHE3 activity and ubiquitination was determined by knockdown in Caco-2bbe cells. The effects of protein kinase A (PKA), the primary mediator of CTX-induced diarrhea, on Nedd4-2 and hNHE3 phosphorylation and their interaction were determined.

RESULTS: The effects of CTX and EPEC were greater in $hNHE3^{int}$ mice than in control wild-type (WT) mice, resulting in greater inhibition of NHE3 activity and increased fluid accumulation in the intestine, the hallmark of diarrhea. Activation of PKA increased ubiquitination of hNHE3 and enhanced interaction of Nedd4-2 with hNHE3 via phosphorylation of Nedd4-2 at S342. S342A mutation mitigated the Nedd4-2–hNHE3 interaction and blocked PKA-induced inhibition of hNHE3. Unlike non-human NHE3s, inhibition of hNHE3 by PKA is independent of NHE3 phosphorylation, suggesting a distinct mechanism of hNHE3 regulation.

CONCLUSIONS: The effects of CTX and EPEC on hNHE3 are amplified, and the unique properties of hNHE3 may contribute to diarrheal symptoms occurring in humans. *(Cell Mol Gastroenterol Hepatol 2022;13:695–716; https://doi.org/10.1016/j.jcmgh.2021.11.006)*

Keywords: Diarrhea; Sodium Transporter; Phosphorylation; Ubiquitination.

Infectious diarrhea caused by enteropathogenic bacteria is a major cause of mortality in young children worldwide and in the wider population within developing countries.[1] The pathogenesis of diarrhea is multifactorial, but infectious diarrhea often results from altered intestinal

transport of electrolytes and fluid.[2] The major Na^+ absorptive mechanism in the intestine is electroneutral NaCl absorption mediated by the Na^+/H^+ exchanger 3 (NHE3), which is functionally linked to a Cl^-/HCO_3^- exchanger. Inhibition of NHE3 activity in the intestine is associated with decreased fluid absorption, which can contribute to diarrheal symptoms.[3] The direct evidence linking NHE3 to diarrhea has come from the studies of mice deficient in NHE3 that develop mild chronic diarrhea and intestinal distention, resulting from retention of alkaline fluid in all intestinal segments.[4] In humans, recessive mutations in the NHE3 gene (*Slc9A3*) cause congenital diarrhea.[5] Diarrhea is one of the most common symptoms in patients with inflammatory bowel disease, including Crohn's disease and ulcerative colitis.[6] Recent genome-wide association studies have established a strong association between ulcerative colitis and the Slc9A3 gene locus, whereas a single nucleotide polymorphism in *Slc9A3* gene is linked to decreased NHE3 activity.[7,8]

Inhibition of NHE3 and the resulting diarrhea can be caused from infection of the gastrointestinal tract by a variety of microorganisms, including *Vibrio cholerae,* enteropathogenic *Escherichia coli* (EPEC), and *Clostridium difficile*. These pathogens produce toxins that alter intestinal transport of electrolytes and fluid.[9] Infection by *Vibrio cholerae* increases Cl^- secretion and decreases Na^+ absorption due to the presence of cholera toxin (CTX) secreted by the bacteria.[10] CTX activates adenylate cyclase, increases 3',5'-cyclic adenosine monophosphate, and activates protein kinase A (PKA). PKA phosphorylates and decreases NHE3 protein abundance in the plasma membrane via stimulation of NHE3 endocytosis, while also preventing delivery of NHE3 to the surface membrane.[11–13] EPEC is a common cause of diarrhea in infants and young children, and the rapid onset of diarrhea in EPEC infections is a result of reduced absorption of ions and solutes.[2,14] EPEC specifically inhibits NHE3 activity via a mechanism requiring the effector protein EspF of a type III secretion system, but the signaling cascade inhibiting NHE3 has not been elucidated.[15]

Ubiquitination is a regulated, post-translational modification that conjugates ubiquitin (Ub) to Lys residues of target proteins and controls their intracellular fate. The covalent ligation of the 76-amino acid peptide Ub to substrate proteins is a highly conserved process that occurs via the sequential action of 3 enzymes: Ub-activation enzyme E1, Ub-conjugating enzyme E2, and Ub ligase E3. E3 ligases play a pivotal role in ubiquitination because these recognize the acceptor proteins and hence dictate the high specificity of the ubiquitination reaction.[16] We have shown recently that NHE3s of human and non-human primates differ from NHE3s of other animals by having a PY (PPxY) motif.[17] A PY motif is necessary for the interaction of a neural precursor cell expressed, developmentally down-regulated 4 (Nedd4) family of E3 Ub enzymes.[18] The presence of a PY motif in human NHE3 (hNHE3) permits ubiquitination of NHE3 by Nedd4-2 in PS120 cells and has also been shown to increase the basal rate of internalization of hNHE3.[17] Recently, ubiquitin-specific peptidase 7 (USP7), USP10, and USP48 have been identified as deubiquitinating enzymes (DUBs) targeting hNHE3.[19,20] Therefore, ubiquitination of hNHE3 is coordinated by the on-reaction by Nedd4-2 and off-reaction by the DUBs.

The use of small animals such as mice and rats as surrogates for humans in scientific studies has advantages because of their small size, short reproductive cycle, and ease of genetic manipulation. However, several components of mouse biological systems are incongruent with those of humans.[21] For instance, small animals such as mice and rats are not perceived to develop diarrhea as often, or as severely, as humans, although a direct comparison of free-living humans exposed to a variety of pathogens that may cause diarrhea and laboratory animals living in a controlled environment is difficult. To overcome such a limitation, we generated a humanized mouse strain expressing hNHE3 in the intestinal epithelial cells (IECs). The goal of this study is to test the hypothesis that ubiquitination of hNHE3 by Nedd4-2 renders hNHE3 more reactive to enteropathogenic agents, thus contributing to increased severity of diarrhea. We used an IEC line and the humanized mouse to establish that hNHE3 displays the unique biochemical property of ubiquitination-dependent regulation, which significantly amplifies the effects of CTX and EPEC, thereby contributing to increased intestinal water loss.

Results

Inhibition of hNHE3 by Forskolin is Greater Than Non-Human NHE3

To demonstrate that the extent of inhibition of hNHE3 is greater than of non-human NHE3, we compared the effect of the adenylate cyclase activator forskolin (FSK) on hNHE3 and rabbit NHE3 (rbNHE3) expressed in Caco-2bbe cells. Na^+/H^+ exchange activity of NHE3 was determined by the rate of initial Na^+-dependent intracellular pH (pH_i) recovery.[17,22] All NHE3 activity measurements were conducted in the presence of 30 μmol/L Hoe-694 or 2 μmol/L dimethyl amiloride, which inhibit endogenous NHE1 and NHE2 activities. Cells expressing hNHE3 and treated with FSK for 30 minutes showed a concentration-dependent inhibition of NHE3 activity. The rate of Na^+/H^+ exchange by hNHE3 was reduced by 24% ± 4% and 55% ± 2% when treated with 1 μmol/L and 10 μmol/L FSK, respectively (Figure 1).

*Authors share co-first authorship.

Abbreviations used in this paper: **ANOVA, analysis of variance; CFTR, cystic fibrosis transmembrane conductance regulator; CTX, cholera toxin; DRA, down-regulated in adenoma; DUB, deubiquitinating enzyme; ENaC, epithelial Na^+ channel; EPEC, enteropathogenic *E coli*; FSK, forskolin; HBSS, Hank's balanced saline solution; hNHE3, human NHE3; IEC, intestinal epithelial cell; IF, immunofluorescence; Nedd4, neural precursor cell expressed, developmentally down-regulated 4; NHE, Na^+/H^+ exchanger; pH_i, intracellular pH; PCR, polymerase chain reaction; PKA, protein kinase A; PKC, protein kinase C; SD, standard deviation; sh, short hairpin; Ub, ubiquitin; USP, ubiquitin-specific peptidase; WT, wild-type.**

Most current article

2352-345X
https://doi.org/10.1016/j.jcmgh.2021.11.006

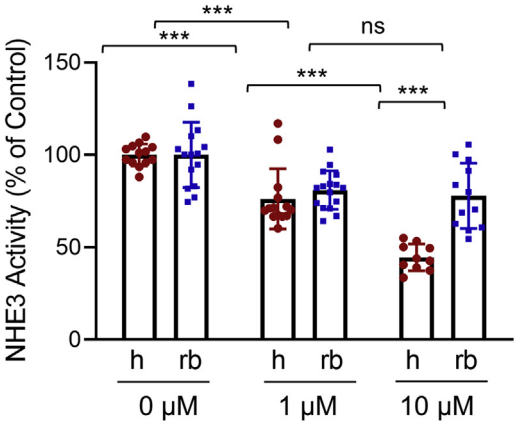

Figure 1. Inhibition of hNHE3 by FSK is greater than non-human NHE3. NHE3 activity was determined in Caco-2bbe/hNHE3 (h) and Caco-2bbe/rbNHE3 (rb) cells treated with 1 or 10 μmol/L FSK for 30 minutes. Results are presented as percent (mean ± SD) of NHE3 activity at 0 μmol/L FSK. Each experimental point represents the rate of initial Na^+-dependent pH recovery of an independent group of cells. Data are representative of 3 experiments. n = 10–16. ***$P < .001$. Statistical analysis was performed by two-way ANOVA with Tukey post hoc test.

In comparison, the activity of rbNHE3 was inhibited by 17% ± 2% by 1 μmol/L FSK, and increasing FSK treatment concentration to 10 μmol/L did not result in further inhibition of rbNHE3 activity (18% ± 3%).

Generation of a Humanized Mouse Expressing Human NHE3

The amplified effects of FSK on hNHE3 suggest that this may contribute to increased diarrheal symptoms. However, diarrhea that results from the loss of water in the intestine cannot be assessed using in vitro systems. To determine whether the presence of hNHE3 increases the severity of diarrhea in humans, we generated a transgenic mouse strain expressing hNHE3 in the IECs. We used the villin promoter to drive the expression of hNHE3 tagged with a VSVG tag at the C-terminus (Figure 2*A*). The transgenic mice were subsequently crossed with *Nhe3*$^{-/-}$ mice, resulting in a mouse strain that expresses hNHE3 in IECs in the absence of mouse NHE3 (Figure 2*B*). This mouse is called hNHE3^{int}. Comparing transgenic expression of hNHE3 with mouse NHE3 by Western blotting showed that hNHE3 expression levels in the jejunum, ileum, and proximal colon are greater compared with mouse NHE3 expression in wild-type (WT) mice (Figure 2*C*). However, because the anti-NHE3 antibody (EM450) was raised against a peptide from hNHE3,[22] it is likely that the amount of mouse NHE3 was underestimated. The mRNA expression levels of the cystic fibrosis transmembrane conductance regulator (CFTR) and the Cl^-/HCO_3^- exchanger DRA (down-regulated in adenoma) were not altered in the IECs of hNHE3^{int} mice (Figure 2*D*). However, NHE2 mRNA expression was decreased in hNHE3^{int} mice (Figure 2*D*), which could be associated with the increased expression of the transgenic hNHE3.

Previous studies have shown that *Nhe3*$^{-/-}$ mice exhibit mild chronic diarrhea and intestinal distention caused by retention of fluid.[4] hNHE3^{int} mice did not show any sign of diarrhea or water accumulation in the intestine, and unlike *Nhe3*$^{-/-}$ mice, formed fecal pellets were present in hNHE3^{int} mice (Figure 2*E*), demonstrating that the expression of hNHE3 has restored the Na^+/H^+ exchange activity in the intestine. In addition, *Nhe3*$^{-/-}$ and WT mice had similar histologic appearances of the intestinal tract with well-formed villi in the small intestine (Figure 2*F*, upper panels) and the absence of hyperplasia and increased immune cell infiltration in the colon that are observed in *Nhe3*$^{-/-}$ mouse colon (Figure 2*F*, lower panels).

It has been shown previously that NHE3 deficiency causes dysbiosis with reduced microbial diversity in the intestine.[23] To determine whether the expression of hNHE3 alters the gut microbiota, we compared the cecal microbiota from WT, *Nhe3*$^{-/-}$, and hNHE3^{int} mice by profiling the major microbial taxonomic groups. As shown previously,[23] there were increased levels of Bacteriodetes and Proteobacteria in *Nhe3*$^{-/-}$ mice, whereas Firmicutes expression was reduced compared with WT mice (Figure 3). This shift in the microbiota composition was largely reversed in hNHE3^{int} mice, and this class level analysis of microbiota, although limited in depth, ascertains the importance of intestinal NHE3 expression for the homeostasis of gut microbiota. The absence of NHE3 is also associated with male infertility due to a defect in acidification of the epididymal fluid so that male *Nhe3*$^{-/-}$ mice are infertile.[24] Although we did not specifically detect the presence of hNHE3 in the male reproductive system of hNHE3^{int} mice, all the hNHE3^{int} male mice that were used for breeding were reproductive, indicating that Na^+/H^+ exchange activity in the epididymal duct was restored in hNHE3^{int} mice.

Effects on Na^+/H^+ Exchange Activity and Na^+-dependent Water Absorption by CTX Are Enhanced in hNHE3^{int} Mice

To determine whether the regulation of hNHE3 and mouse NHE3 differs in vivo, we assessed the effects of FSK on NHE3 activity by injecting FSK or dimethyl sulfoxide into a small segment of mouse ileum ligated on both ends to form a closed loop (Figure 4*A*). The mice were kept for 90 minutes under anesthesia on a warming bed, with the abdomen covered with a moist towel. Mice were then euthanized, and intestinal villi were isolated for the measurement of NHE3 activity as previously described.[25] The basal activity of hNHE3 was higher than that of mouse NHE3 in WT mice, which correlates with increased expression of hNHE3 than the endogenous level in control mice. However, FSK resulted in significantly greater inhibition of NHE3 activity in hNHE3^{int} mice compared with that in WT mice (Δ82.3% for hNHE3^{int} vs Δ43.4% for WT), so that hNHE3 activity in the presence of FSK was lower than mouse NHE3 activity (Figure 4*A*).

Na^+ absorption by NHE3 in the IECs facilitates transepithelial water absorption across the intestinal epithelial barrier.[3] Hence, NHE3 inhibition leads to decreased

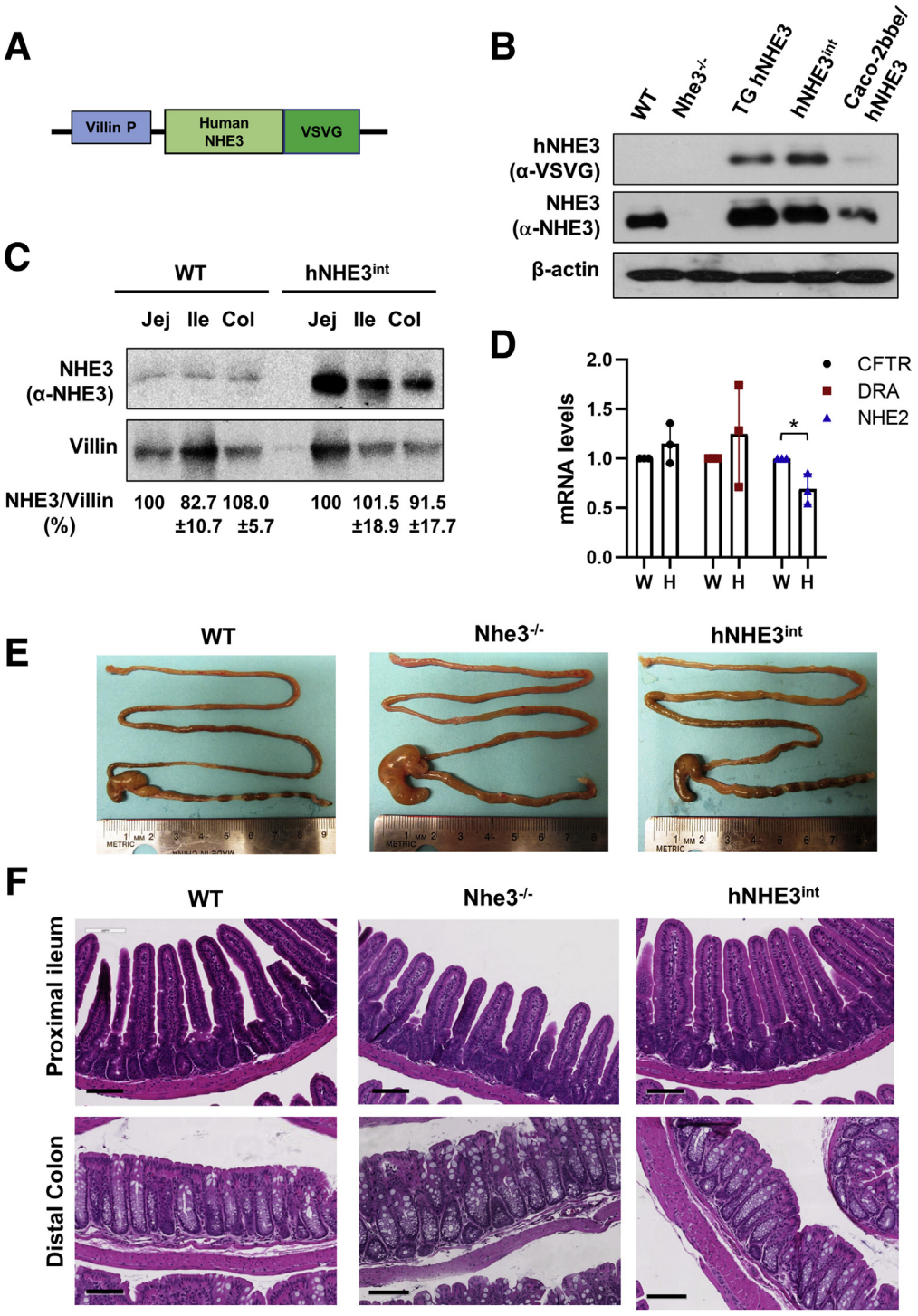

Figure 2. Generation of humanized mice expressing hNHE3 in mouse intestine. (*A*) Schematic map of the transgenic construct consists of a villin gene promoter (P), a VSVG-tag, and hNHE3 gene. The drawing is not to scale. (*B*) NHE3 expression was determined in jejunum mucosal lysates of WT mice, NHE3 knockout (Nhe3$^{-/-}$) mice, transgenic mice expressing both human and mouse NHE3 (TG hNHE3), and hNHE3^{int} mice expressing only human NHE3 in intestinal tissue. Cell line Caco-2bbe transfected with human NHE3 was included as a positive control. Western blots were performed using P5D4 anti-VSVG antibody and EM450 polyclonal NHE3 antibody to detect hNHE3 and total NHE3, respectively. β-actin was used as loading control. (*C*) Western blot comparing mouse NHE3 in WT and hNHE3 in hNHE3^{int} mouse intestine using EM450 anti-NHE3 antibody. Col, proximal colon; Ile, ileum; Jej, jejunum. (*D*) mRNA expression of CFTR, DRA, and NHE2 in the small intestinal mucosa was determined by quantitative real-time PCR of WT and hNHE3^{int} mice. Relative expression is presented as fold changes relative to expression level in WT mice. Results are mean ± SD (n = 3). *$P < .05$ by unpaired *t* test. (*E*) Representative appearance of the intestinal tract of WT, *Nhe3*$^{-/-}$, and hNHE3^{int} mice. (*F*) Histology of proximal ileum and distal colon of WT, *Nhe3*$^{-/-}$, and hNHE3^{int} mice are shown. Bar, 100 mm. Results are representative of 3 independent experiments.

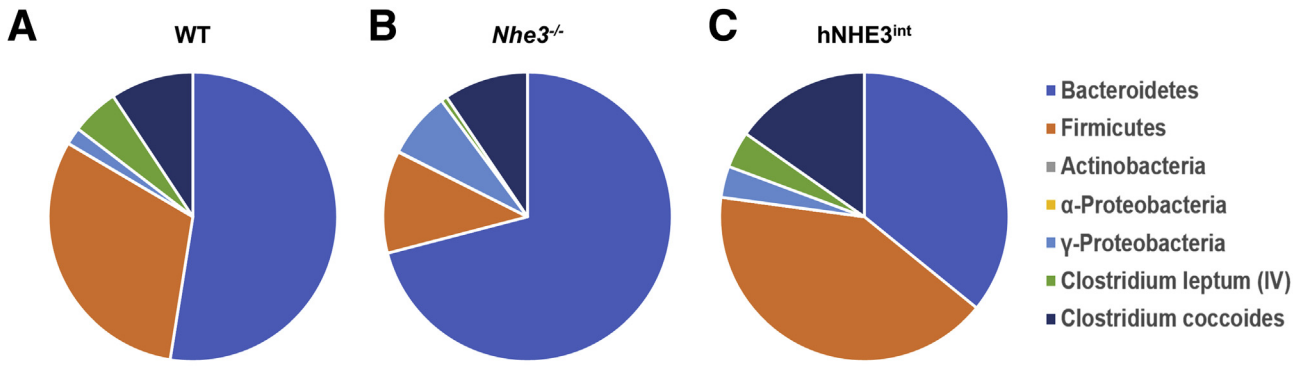

Class level analysis of cecum microbiota of *Nhe3*$^{-/-}$ and hNHE3^{int} mice

	WT		Nhe3$^{-/-}$		hNHE3^{int}		p value (n>4)		
	Mean (%)	SEM	Mean (%)	SEM	Mean (%)	SEM	WT vs Nhe3$^{-/-}$	WT vs hNHE3^{int}	Nhe3$^{-/-}$ vs hNHE3^{int}
Bacteroidetes	52.52	3.54	70.95	5.30	35.85	3.79	0.5145	0.0001*	0.0004*
Firmicutes	30.94	1.83	11.44	0.74	41.31	5.86	<0.0001*	0.0075*	<0.0001*
Actinobacteria	0.01	0.00	0.06	0.01	0.01	0.00	0.0018*	0.1015	0.0007*
α-Proteobacteria	0.01	0.00	0.01	0.00	0.01	0.00	0.0669	0.3411	0.1958
γ-Proteobacteria	1.92	0.48	7.41	0.44	3.49	0.62	<0.0001*	0.0703	0.0005*
Clostridium leptum (IV)	5.31	0.51	0.68	0.03	4.08	0.65	<0.0001*	0.0410*	<0.0001*
Clostridium coccoides	9.30	1.28	9.46	1.53	15.26	1.83	0.2981	0.0051*	0.0025*

Figure 3. Microbial profiles of cecum contents of WT, Nhe3$^{-/-}$, and hNHE3^{int} mice. Cecum contents of (*A*) WT (n = 5), (*B*) *Nhe3*$^{-/-}$ (n = 4), and (*C*) hNHE3^{int} (n = 5) mice were collected under sterile conditions, and bacterial genomic DNA was extracted. Microbial profiles were determined by real-time PCR using specific primers (Table 1) as described previously.[23] Data were analyzed by two-way ANOVA. *$P < .01$. Data are representative of 2 experiments. SEM, standard error of the mean.

Na^+ absorption, which causes luminal water accumulation, a proxy for diarrhea. CTX treatment for 5 hours resulted in accumulation of fluid in the intestinal loop of WT mice as evidenced by increased weight-to-length ratios (Figure 4*B*). Although increased water accumulation in the intestinal loop was evident in both mouse strains, CTX treatment almost doubled the effect in hNHE3^{int} mice compared with WT mice. However, CTX can cause both decreased absorption by NHE3 and increased secretion by CFTR, resulting in fluid accumulation.[10] To evaluate whether the CFTR-dependent secretory activity was altered, fluid accumulation in an intestinal loop was determined in the presence of NHE3 inhibitor S3226. The rate of fluid accumulation with NHE3 inhibited was comparable between WT and hNHE3^{int} mice (Figure 4*C*), suggesting that the transgenic hNHE3 expression did not significantly alter CFTR function. However, we could not assess NHE3-dependent fluid absorption by using the closed-loop model in the presence of a CFTR inhibitor, because attempts to do so resulted in shrinkage of the intestinal segment. We hypothesize that this was due to reabsorption of entire luminal fluid in the absence of any secretory activity. To circumvent this limitation, we used the in vivo perfusion system in which a small loop of intestine of an anesthetized mouse is perfused in a recirculating manner.[26] Mice were administered a CFTR inhibitor, CFTRinh-172, intraperitoneally 1 hour before the start of perfusion to block CFTR-mediated secretion. Similar treatment was shown to block about 90% of CFTR activity.[27,28] The basal rate of water absorption was greater in hNHE3^{int} mice than WT mice (Figure 4*D*), which is consistent with the higher expression levels of hNHE3 versus mouse NHE3. Administration of CTX in the perfusion buffer resulted in a significant decrease in the rate of water absorption in both strains. Importantly, CTX decreased the rate of water absorption by 50% in hNHE3^{int} intestine compared with 27% in WT intestine. As such, the rate of water absorption with CTX in hNHE3^{int} intestine was significantly lower than what was observed in the WT intestine (Figure 4*D*). We confirmed the differential effects on water absorption by determining the antiporter activity in isolated villi from the closed intestinal loops. The effect of CTX on the hNHE3 activity of hNHE3^{int} mouse villi was significantly greater compared with mouse NHE3 activity (Δ76.8% for hNHE3^{int} vs Δ49.1% for WT) (Figure 4*E*).

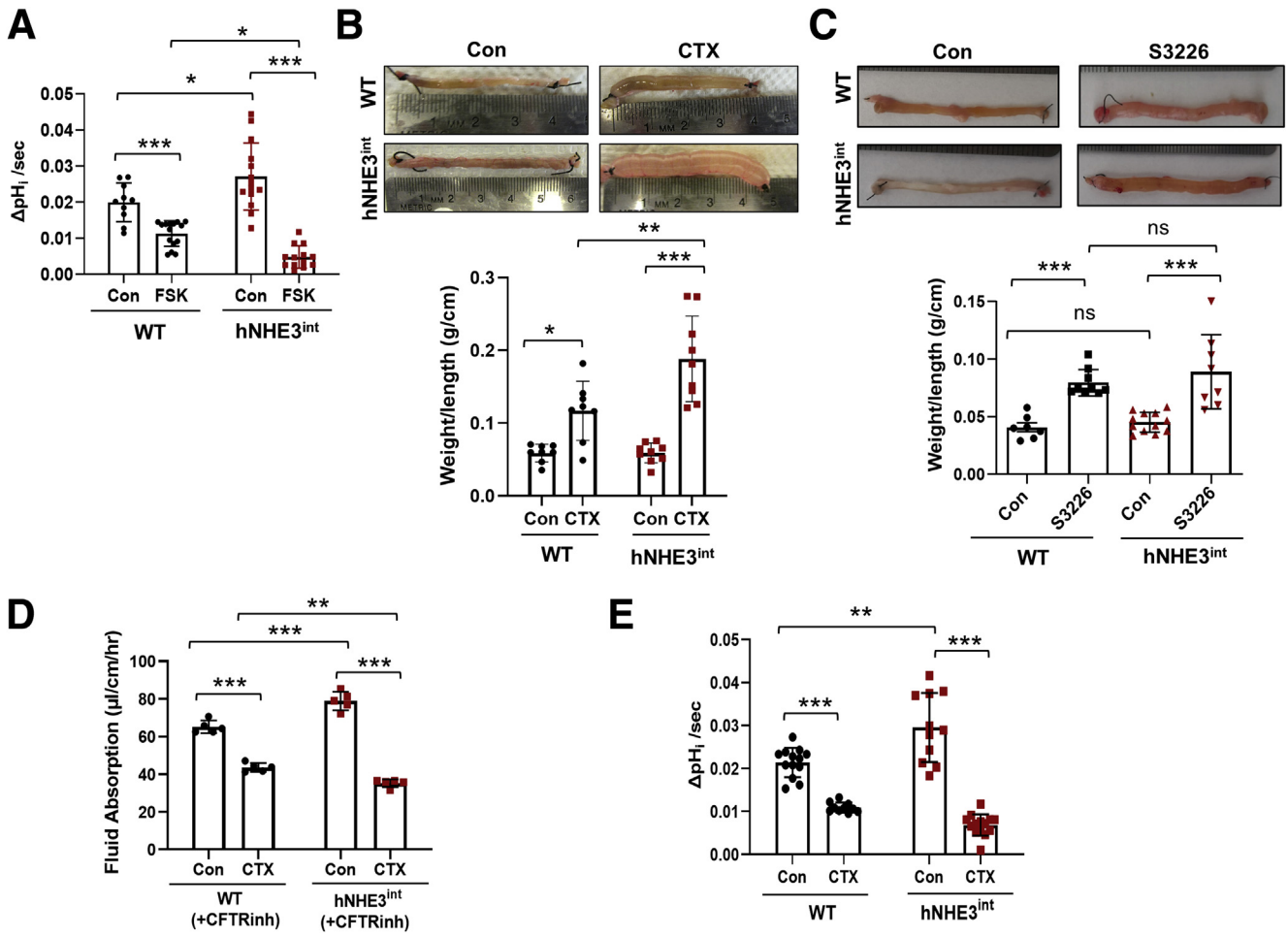

Figure 4. CTX-induced inhibition of NHE3 and water loss are greater in humanized mice. (*A*) Two adjacent segments of WT and hNHE3^{int} ileum were ligated on both ends. One segment was administered with 10 μmol/L FSK and the other with the same volume of dimethyl sulfoxide as the control for 90 minutes. Villi were isolated, and the initial rate of Na^+-dependent intracellular pH recovery was determined. n $\geq$ 10. *$P < .05$, ***$P < .001$. (*B*) Closed intestinal loops were injected with CTX (10 μg in 100 μL HBSS) or the same volume of HBSS (Con) as described above. Five hours later, weight (g) and length (cm) of the ligated segments were measured. *Upper*, representative appearance of ligated loops is shown. *Lower*, ratios of weight/length are presented. n = 8 for WT, n = 9 for hNHE3^{int} mice. **$P < .01$, ***$P < .001$. (*C*) Fluid accumulation in closed ileal loops was determined in the presence of NHE3 inhibitor S3226. *Upper*, representative images of closed intestinal loops. *Lower*, ratios of weight/length (mean ± SD). n = 8–12. ***$P < .001$. Data are representative of 2 independent experiments. (*D*) Fluid absorption in the mouse ileum was determined by in vivo perfusion system as described in the Methods section in the presence of the CFTR inhibitor, CFTRinh-172. Rates of fluid absorption in the absence (Con) or presence of CTX are shown. n = 5. **$P < .01$, ***$P < .001$. (*E*) NHE3 activities were determined in isolated villi from the closed intestinal segments treated with CTX or HBSS. n $\geq$ 9. **$P < .01$, ***$P < .001$. Statistical significance was determined by two-way ANOVA with Tukey post hoc test.

Inhibition of hNHE3 Is Dependent on Nedd4-2

Our previous study showed that hNHE3 uniquely interacts with Nedd4-2, which ubiquitinates and internalizes hNHE3 under basal conditions.[17] We therefore hypothesized that the increased reactivity of hNHE3 in response to CTX is a result of Nedd4-2–dependent regulation of hNHE3. To test the hypothesis, we examined the effect of loss of Nedd4-2 function by knocking down Nedd4-2 in Caco-2bbe cells. Figure 5*A* shows that Nedd4-2–specific lentiviral short hairpin (sh) RNA, shNedd4-2, led to decreased Nedd4-2 protein expression compared with cells treated with scrambled control shRNA (shCon). Importantly, silencing Nedd4-2 expression blocked FSK-induced inhibition of hNHE3 (Figure 5*B*). Our previous study demonstrated that the hNHE3–Nedd4-2 interaction requires the presence of ^{723}PPNYDEE^{729} motif, called the extended PY motif (ePY), in hNHE3.[17] To further assess the role of Nedd4-2, we expressed hNHE3 with the ePY motif mutated to Ala (ePY^{mut}) in Caco-2bbe cells. Consistent with the effect of Nedd4-2 knockdown, Nedd4-2/ePY^{mut} rendered hNHE3 nonresponsive to FSK (Figure 5*C*).

If hNHE3 inhibition is dependent on Nedd4-2, we postulated that ubiquitination of hNHE3 must be increased by CTX treatment. Therefore, we immunoprecipitated hNHE3 from Caco-2bbe cells before or after FSK treatment. FSK induced a significant increase in ubiquitination levels of

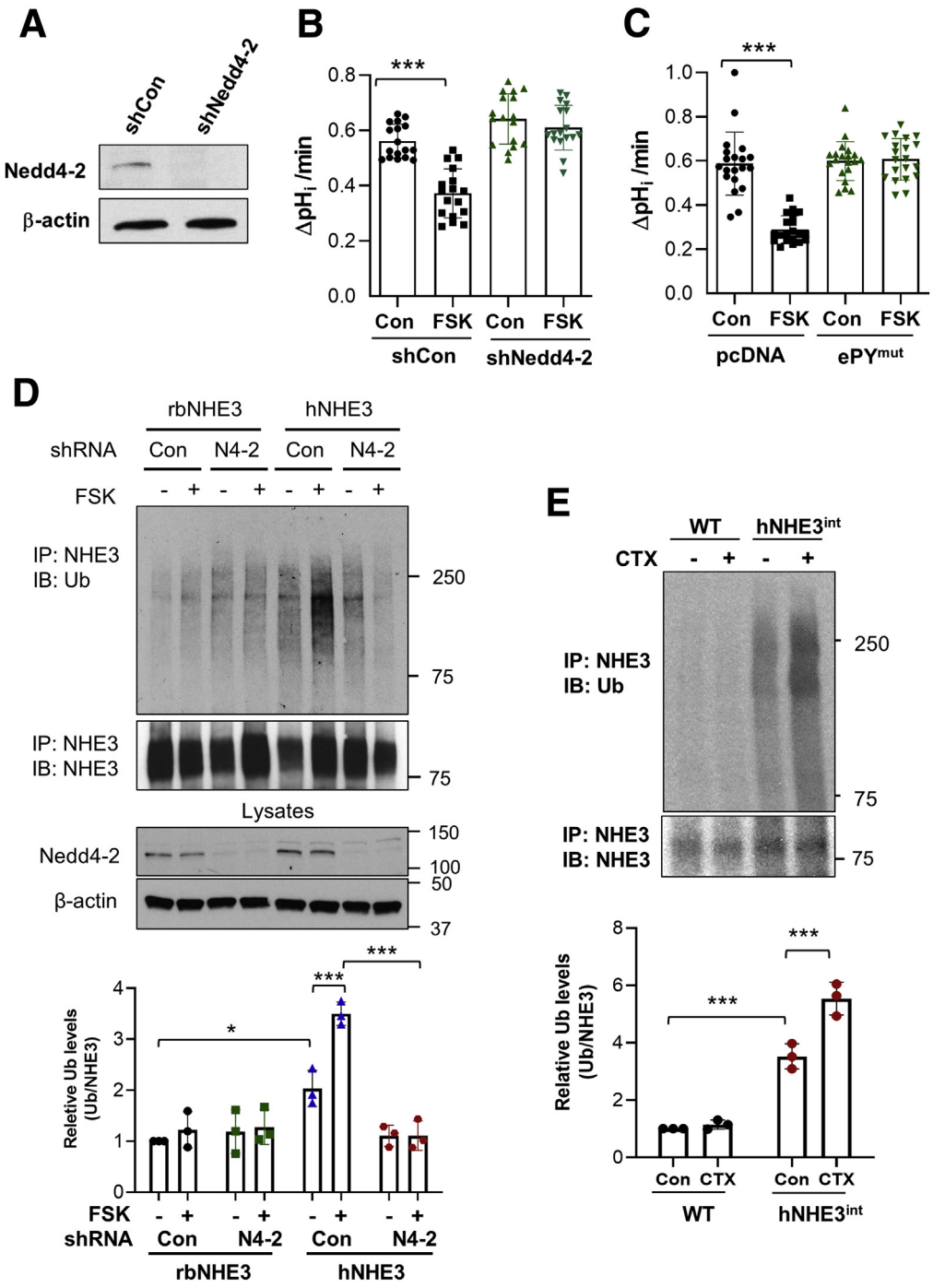

Figure 5. Inhibition of hNHE3 by FSK requires Nedd4-2. (*A*) Nedd4-2 expression was stably silenced in Caco-2bbe cells by using lentiviral shNedd4-2. Scrambled shRNA (shCon) was used as a control. Expression of endogenous Nedd4-2 was determined by Western blotting using anti-Nedd4-2 antibody. Representative blots from more than 3 independent experiments are shown. (*B*) Caco-2bbe/hNHE3 cells stably transduced with shNedd4-2 or shCon were treated with FSK or equal volume of dimethyl sulfoxide (Con) for 30 minutes. NHE3 activity was determined as the rate of Na^+-dependent pH_i recovery. Results are presented as mean ± SD. n = 17. ***$P < .001$. (*C*) Caco-2bbe/hNHE3 cells transfected with pcDNA control or pcDNA/Nedd4-2-ePY^{mut} were treated with FSK as described above. n = 20. ***$P < .001$ by one-way ANOVA. (*D*) Caco-2bbe/rbNHE3 and Caco-2bbe/hNHE3 cells transduced with shNedd4-2 or shCon were treated with 10 μmol/L FSK for 30 minutes. NHE3 was immunoprecipitated with P5D4 antibody, and ubiquitination of NHE3 was determined by using P4D1 anti-Ub antibody. The panel below shows immunoprecipitated NHE3 blotted with EM450 antibody. Knockdown of Nedd4-2 is shown in the lower panel with β-actin as control. Representative blots from 3 independent experiments are shown. The lower graph shows the quantification of Ub normalized to NHE3 immunoprecipitated. *$P < .05$, ***$P < .001$ by two-way ANOVA Tukey post hoc test. (*E*) Mouse NHE3 and hNHE3 were immunoprecipitated from intestinal mucosal lysates of WT and $hNHE3^{int}$ mice, respectively, with EM450 anti-NHE3 antibody. Ubiquitination levels of NHE3 were determined and normalized to the amount of NHE3 immunoprecipitated. Quantification from 3 independent experiments is shown on the right. ***$P < .001$ by two-way ANOVA.

hNHE3, which was blocked by shNedd4-2 (Figure 5*D*). In comparison, FSK or Nedd4-2 knockdown did not alter rbNHE3 ubiquitination, consistent with the previous finding in PS120 cells that rbNHE3 or rat NHE3 is not ubiquitinated by Nedd4-2.[17] To determine whether FSK-induced hNHE3 ubiquitination occurs in vivo, we immunoprecipitated hNHE3 and mouse NHE3 from hNHE3^{int} and WT mouse intestine, respectively. Consistent with the results observed in Caco-2bbe cells, CTX significantly increased hNHE3 ubiquitination levels (Figure 5*E*). In comparison, the basal ubiquitination levels of mouse NHE3 were significantly lower and FSK had no effect.

Previous studies have shown that PKA-mediated inhibition of NHE3 involves internalization of NHE3 from the brush border membrane.[12] To assess whether there is a difference in endocytic retrieval of hNHE3 and rbNHE3, we determined NHE3 abundance at the apical membrane of Caco-2bbe cells by surface biotinylation.[26] FSK decreased surface membrane protein abundance of both rbNHE3 and hNHE3, but the effect was greater on hNHE3 than rbNHE3 (Figure 6*A*). Moreover, FSK-induced effect on hNHE3 surface abundance was ablated by shNedd4-2, whereas no difference was observed on rbNHE3 (Figure 6*A*), further demonstrating the importance of Nedd4-2 in hNHE3 regulation. The differential effects on NHE3 internalization by CTX in Caco-2 cells were confirmed by immunofluorescence (IF) confocal microscopic analysis of the ligated intestinal loops of mice. In WT mice, CTX treatment decreased brush border membrane expression of NHE3, causing the appearance of NHE3 in the subapical compartment (Figure 6*B*, left panels). In comparison, the retrieval of hNHE3 from the brush border membrane was significantly enhanced in the hNHE3^{int} mice (Figure 6*B*, right panels), indicating that the increased inhibition of hNHE3 activity results in part from enhanced endocytosis of hNHE3 protein.

Inhibition of hNHE3 by EPEC Is Nedd4-2 Dependent

EPEC is a common cause of diarrhea in infants and young children, and the rapid onset of diarrhea in EPEC infections is a result of reduced absorption of ions and solutes.[2,14] EPEC specifically inhibits NHE3 activity via a mechanism requiring the effector protein EspF of a type III secretion system.[15] To assess whether the Nedd4-2 dependence of hNHE3 extends beyond CTX-mediated inhibition, we compared the effects on EPEC on hNHE3 and rbNHE3 in Caco-2bbe cells. Cells were treated with Luria Broth or a commensal strain EFC-1, which did not alter the basal Na^+/H^+ exchange activities of hNHE3 or rbNHE3 (Figure 7*A*).[29] However, when treated with the enteropathogenic strain EPEC, the extent of inhibition was significantly greater for hNHE3 compared with rbNHE3 (Figure 7*B*). In cells expressing hNHE3, the NHE3 activity was inhibited by 60.8% compared with 38.5% inhibition observed for rbNHE3. Moreover, EPEC-mediated inhibition of hNHE3 activity was abolished by knockdown of Nedd4-2 (Figure 7*C*), and EPEC failed to regulate hNHE3/ePY^{mut} (Figure 7*D*), indicating that the regulation of hNHE3 by EPEC is Nedd4-2 dependent. To determine whether hNHE3 ubiquitination is induced by EPEC, hNHE3 was immunoprecipitated and blotted for Ub. Figure 7*E* shows that EPEC increased ubiquitination levels of hNHE3. It is noteworthy that the mechanism of how the EPEC effector modulates NHE3 activity is not clear.[15] EPEC is known to regulate protein kinase C (PKC), but there is also prevalent information that heat-stable enterotoxin secreted by bacteria strains, such as enterotoxigenic *E coli*, regulate protein kinase G.[30,31] Therefore, we evaluated the effects of a pan-PKC inhibitor Gö6983 and PKG inhibitor AP-C5 on EPEC-mediated NHE3 regulation in Caco-2bbe cells.[32] Inhibition of PKC blocked EPEC-induced NHE3 inhibition (Figure 7*F*), and PKG inhibition did not, suggesting that EPEC regulates NHE3 via a PKC-dependent mechanism.

We next compared the effect of EPEC on WT and hNHE3^{int} mice by oral administration of EPEC daily for 7 days. We determined body weight, water intake, and fecal water content daily. Water intake or body weight was not significantly changed during the EPEC treatment in both WT and hNHE3^{int} mice (Figure 8*A* and *B*). However, there was a moderate trend that fecal water contents in hNHE3^{int} mice were higher than in WT mice during EPEC treatment, reaching statistical significance on days 1, 6, and 7 compared with WT mice (Figure 8*C*).

The moderate difference between hNHE3^{int} and WT mice could have been due to inefficient colonization of EPEC in the mouse gut, because the adherence and colonization of EPEC in mouse intestine are debatable.[33,34] Therefore, we assessed the effect of EPEC on intestinal water absorption by using the in vivo perfusion system.[26] Previous studies have shown that EPEC infection of cultured human colonic T84 cells attenuates secretagogue-induced net ion transport without an effect on Cl^- secretion.[35] Therefore, we determined the effect of EPEC infection without CFTR inhibition. The average rate of fluid absorption in WT was decreased by 48% in the presence of EPEC in the perfusion buffer. In comparison, EPEC resulted in 82% decrease in hNHE3^{int} mice (Figure 8*D*). To directly determine the effect of EPEC on NHE3 activity, EPEC was administered into closed intestinal loops, and villi were isolated after 90 minutes to determine the antiporter activity. The extent of decrease in NHE3 activity was 30% and 62% for WT and hNHE3^{int} mice, respectively (Figure 8*E*), confirming the heightened effects on hNHE3.

Regulation of hNHE3 by PKA Is Dependent on Phosphorylation of Nedd4-2

The results thus far have highlighted the importance of Nedd4-2 in enforcing hNHE3 inhibition. Nedd4-2 contains 4 WW domains (protein-protein interaction domains containing 2 conserved tryptophan residues) that bind PY motifs.[36] To identify a WW domain interacting with hNHE3, each WW domain expressed as a glutathione S transferase fusion protein was used to pulldown hNHE3 from Caco-2bbe/hNHE3 cell lysate. Only the third WW (WW3) bound

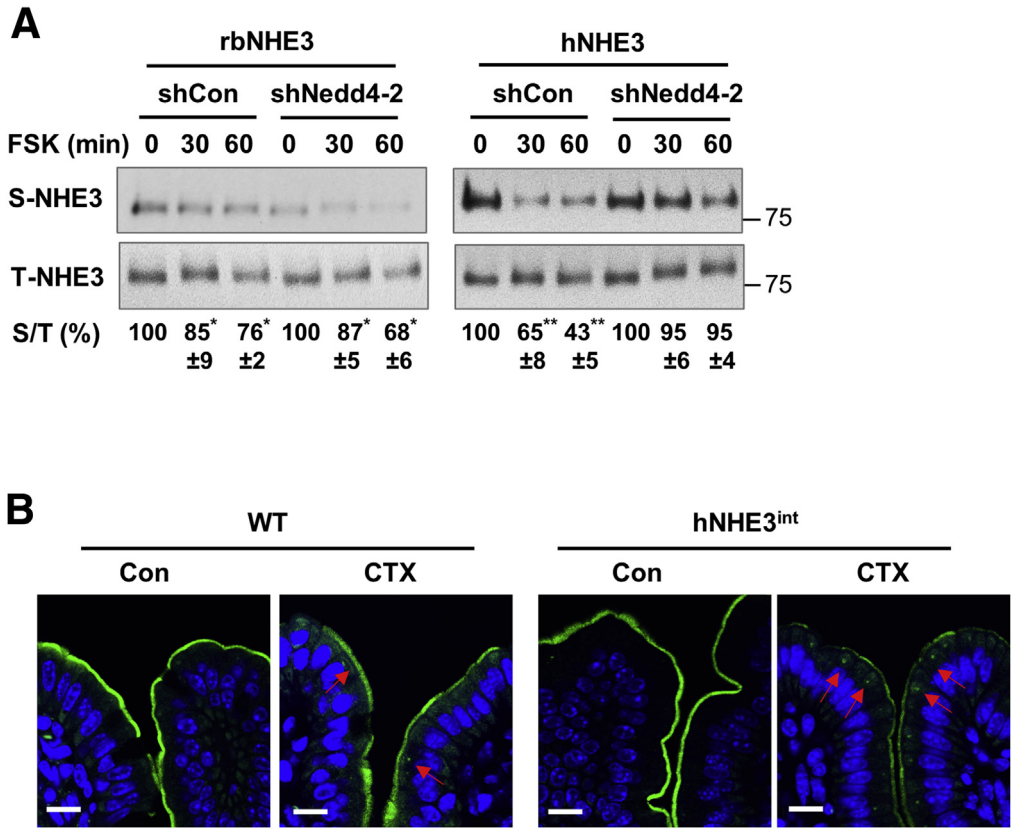

Figure 6. Internalization of hNHE3 by PKA is dependent on Nedd4-2. (*A*) NHE3 expression at the apical membrane of Caco-2bbe cells treated with FSK was determined by surface biotinylation. Surface NHE3 expression was normalized to total NHE3 expression. Relative surface-to-total NHE3 ratios with the result in untreated cells set at 100% (mean ± SD) are shown below the blots. n = 3. *$P < .05$, **$P < .01$ compared with corresponding controls by one-way ANOVA. (*B*) Cellular localization of NHE3 in CTX or control treated ileal tissues was determined by confocal IF microscopy. Representative immunolabeling of NHE3 (*green*) and DAPI (*blue*) are shown. Results are representative 2 independent experiments with 4 mice per group. *Arrows* indicate internalized NHE3. Scale bar: 10 μm.

to hNHE3 (Figure 9*A*), indicating that hNHE3 interacts with Nedd4-2 via WW3.

We next determined whether FSK regulates the interaction between hNHE3 and Nedd4-2. We assessed the localization of hNHE3–Nedd4-2 interaction by confocal IF microscopy. Under basal conditions, hNHE3 was localized at the apical membrane (identified by WGA) with relatively weak colocalization with Nedd4-2 (Figure 9*B*). Treatment with FSK for 5 or 10 minutes decreased hNHE3 at the apical membrane, whereas colocalization of hNHE3 and Nedd4-2, quantified by determining Pearson's coefficient, intensified. These results demonstrate that FSK increases the interaction of Nedd4-2 with hNHE3.

Previous studies have shown that Nedd4-2 is a substrate for phosphorylation by PKA at S342 and S448, and phosphorylation modulates Nedd4-2 interaction with its substrates.[37,38] To determine phosphorylation of Nedd4-2, Caco-2bbe cells were treated with FSK, and phosphorylation of endogenous Nedd4-2 at S342 and S448 was detected using phospho-specific antibodies. FSK increased phosphorylation of Nedd4-2 at S342 as early as 10 minutes but did not affect phosphorylation at S448 (Figure 9*C*, left panels). Similar results were obtained in SK-CO15 cells (Figure 9*C*, right panels). To determine whether FSK increases the interaction of p-Nedd4-2 with hNHE3, we performed co-immunoprecipitation of hNHE3 and Nedd4-2 from Caco-2bbe cells treated with FSK. We observed increased amounts of pS342-HA-Nedd4-2 co-immunoprecipitated with hNHE3 after FSK treatment (Figure 9*D*, first row). Because the anti-pS342-Nedd4-2 antibody was not suitable for IF staining, we could not confirm the interaction of pS342-HA-Nedd4-2 with hNHE3 by IF microscopy. Surprisingly, we did not detect a change when the immunocomplexes were blotted using anti-Nedd4-2 antibody (Figure 8*D*, second row). However, this could be related to the limitation of co-immunoprecipitation that cannot detect region-specific interaction.

To determine whether Nedd4-2 phosphorylation is important for its interaction with hNHE3, we sought to express HA-Nedd4-2 with S342A mutation. Surprisingly, the expression levels of S342A-Nedd4-2 mutant were markedly lower than WT HA-Nedd4-2 in both Caco-2bbe and SK-CO15 cells (Figure 10*A*). Decreased expression levels were also observed for S448A and S342A/S448A mutation (Figure 10*A*). Therefore, we determined whether the S342A and S448A mutations alter protein stability by determining

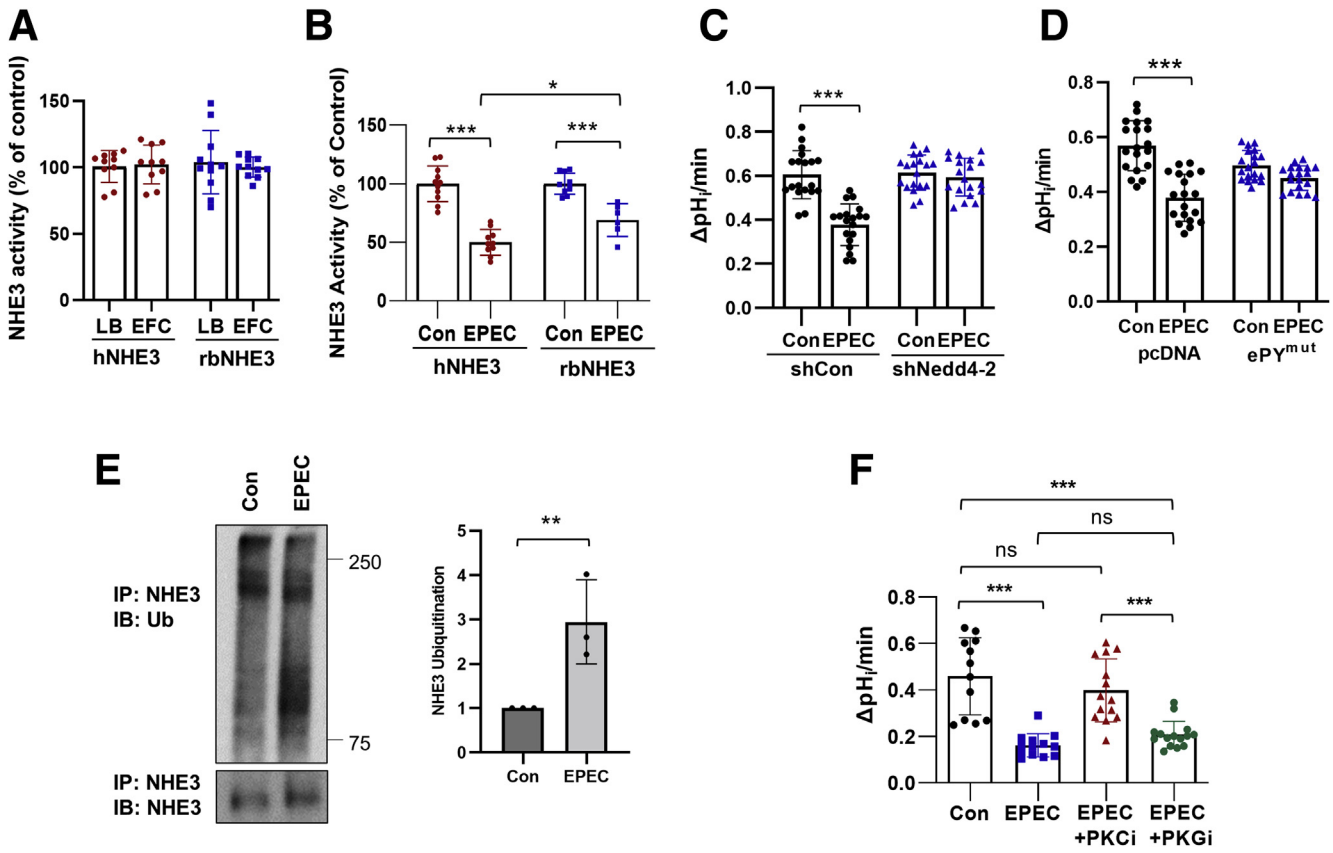

Figure 7. Inhibition of NHE3 by EPEC is greater for hNHE3. (*A*) NHE3 activity is not altered by the commensal EFC-1 strain. NHE3 activity was determined in Caco-2bbe/hNHE3 and Caco-2bbe/rnNHE3 cells treated with EPC or LB medium (control) for 90 minutes. n = 10. (*B-C*) NHE3 activity was determined in cells treated with EPEC or EFC-1 (Con) for 90 minutes. n = 20. ***$P < .001$. (*D*) Caco-2bbe/hNHE3 cells transfected with pcDNA control or pcDNA/Nedd4-2-ePY^{mut} were treated with EPEC as described above. n = 20. ***$P < .001$ by one-way ANOVA. (*E*) Ubiquitination of hNHE3 was determined in Caco-2bbe cells treated with EPEC. hNHE3 was immunoprecipitated and blotted with anti-Ub antibody P5D1. Lower panel shows immunoprecipitated hNHE3. Graph on the right represents quantification of Ub/hNHE3. **$P < .01$. Representative of 2 independent experiments with 3 mice per group. (*F*) Activity of hNHE3 in Caco-2bbe cells was determined in presence of pan-PKC inhibitor (PKC_i) Gö6983 or PKG inhibitor (PKG_i) AP-C5. n = 12–15. ***$P < .001$. Statistical analysis was performed by two-way ANOVA with Tukey post hoc test.

the steady-state protein expression in the presence of translation inhibitor cycloheximide. The expression level of Nedd4-2 was unaltered over 4 hours as shown in Figure 10*B*. By contrast, the rates of decay of S342A and S448A mutants were more rapid, resulting in significant loss of the proteins in 4 hours. As a result, the expression level of S342A mutant was significantly lower than that of endogenous Nedd4-2 expression (Figure 10*C*) and could not be used as a dominant negative. As an alternative to the colonic epithelial cell lines, we used PS120 cells where the expression level of the S342A mutant was similar to that of WT HA-Nedd4-2 (Figure 10*D*). PS120 cells were co-transfected with hNHE3 and HA-Nedd4-2 variants, and co-immunoprecipitation was performed to determine whether the S342A mutation alters the hNHE3–Nedd4-2 interaction. Results in Figure 10*E* demonstrate that the interaction of the S342A mutant with hNHE3 was impaired compared with WT Nedd4-2, indicating that phosphorylation at S342 facilitates their interaction. To test for the functional importance of S342 phosphorylation, the effect of FSK on hNHE3 was determined. As expected, FSK inhibited hNHE3 activity in cells transfected with pcDNA or HA-Nedd4-2 (Figure 10*F*). In contrast, inhibition of hNHE3 by FSK was blocked by the S342A mutant, demonstrating that phosphorylation of Nedd4-2 at S342 is functionally important for hNHE3 regulation.

Inhibition of hNHE3 by FSK Is Independent of NHE3 Phosphorylation at S552

A series of studies have demonstrated that phosphorylation at S552 and S605 of rat NHE3 is important for NHE3 endocytosis and inhibition of NHE3 activity.[11,39] However, it is not known whether phosphorylation at S552 and S605 affects the interaction of Nedd4-2 with hNHE3 or influences phosphorylation of Nedd4-2 by PKA. To this end, we freshly expressed WT hNHE3 and hNHE3 carrying S552A or S605A mutation in Caco-2bbe cells. Cells were treated with FSK, and phosphorylation of hNHE3 was determined using phospho-specific NHE3 antibodies that recognize NHE3

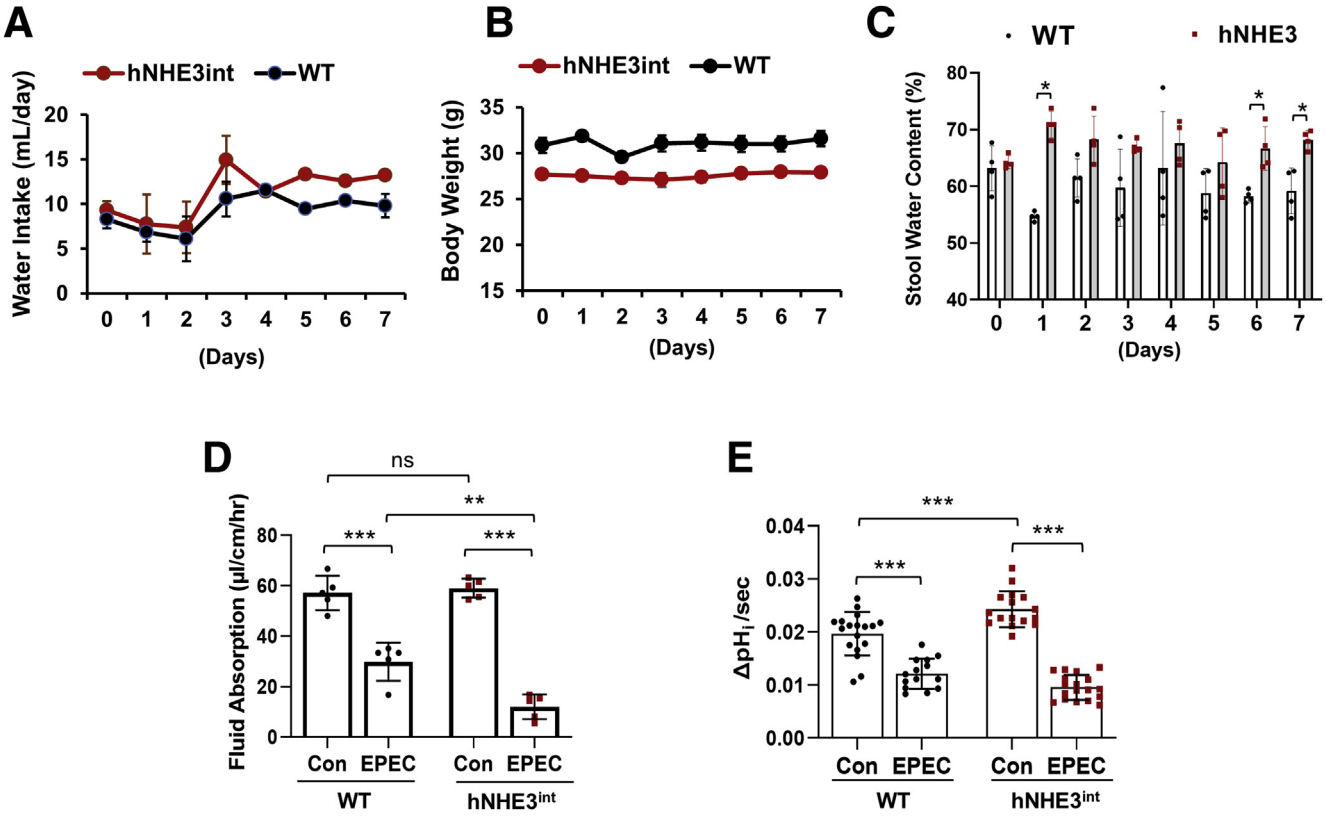

Figure 8. EPEC treatment of hNHE3^{int} and WT mice. Mice were treated with 100 μL of 2 $\times$ 10^6 EPEC via oral gavage for 7 days. Body weight, water consumption, and stool samples were monitored daily over the treatment period at the same time of day. One pretreatment measurement was taken on day 0. (*A*) Water intake was measured by weighing the water bottles daily and calculating the amount of water consumed each day, divided by the number of mice held within a single cage (mL/day). (*B*) Body weight of mice (g) was measured throughout the treatment period. (*C*) Stool water content was measured by taking a daily stool sample, weighing the sample at time of collection (wet weight), heating the sample overnight on a heating block, and re-weighing the dry weight of the sample the following day. Water content was calculated by dry weight divided by wet weight and shown as a percentage. Data are representative of 2 independent experiments with 4–5 mice per group. Results are represented as ± SD. *$P < .05$. Data were analyzed by repeated-measures two-way ANOVA. (*D*) Rate of fluid absorption (mean ± SD) was determined in intestinal sections of WT and hNHE3^{int} mouse perfused with buffer containing EPEC or EFC-1 bacteria. n = 5. **$P < .01$, ***$P < .001$. (*E*) Villi were isolated from the ligated ileal segments for measurement of NHE3 activity (mean ± SD). n > 14–25. ***$P < .001$ by two-way ANOVA Tukey post hoc test.

only if phosphorylated at S552 or S605.[40] Phosphorylation of hNHE3 at S552 was increased by FSK (Figure 11*A*, lane 1 versus lane 2), but as expected, no signal was detected in hNHE3 with S552A mutation (Figure 11A, lanes 3 and 4). Because S552 was unaltered in the S605A mutant, increased phosphorylation at S552 was observed (Figure 11*A*, lane 5 versus lane 6). However, the anti-pS605 antibody failed to show any signal. It is not clear whether S605 of hNHE3 is not a site of phosphorylation, or the antibody does not cross-react with hNHE3. Phosphorylation at S552 by PKA was confirmed in hNHE3^{int} mouse intestine exposed to CTX (Figure 11*B*). To determine the functional role of pS552 and pS605, the effect of FSK on the antiporter activity was determined. As shown earlier, the activity of WT hNHE3 was reduced by FSK, but surprisingly, FSK also inhibited the activities of S552A and S605A mutants (Figure 11*C*). These results suggested that PKA-induced regulation of hNHE3 is independent of phosphorylation at S552 and S605. To determine whether the mutations in hNHE3 alter the interaction with Nedd4-2, we performed co-immunoprecipitation of hNHE3 and Nedd4-2. In all cells, FSK increased phosphorylation of Nedd4-2 at S342 (Figure 11*D*, lower panels), indicating that hNHE3 phosphorylation at S552 and S605 does not alter Nedd4-2 phosphorylation. Moreover, co-immunoprecipitation of pS342-Nedd4-2 with hNHE3 proteins was increased by FSK in all cell lines (Figure 11*D*, upper panels). To determine whether hNHE3 mutants are still ubiquitinated, we transiently expressed HA-Ub and immunoprecipitated hNHE3. Results shown in Figure 11*E* depict that FSK similarly increased ubiquitination levels of hNHE3 variants, demonstrating that phosphorylation at S552 and S605 is not important for Nedd4-2 docking or ubiquitination of hNHE3. Because of the previous evidence demonstrating the importance of phosphorylation of non-human NHE3s, these data demonstrate a distinct

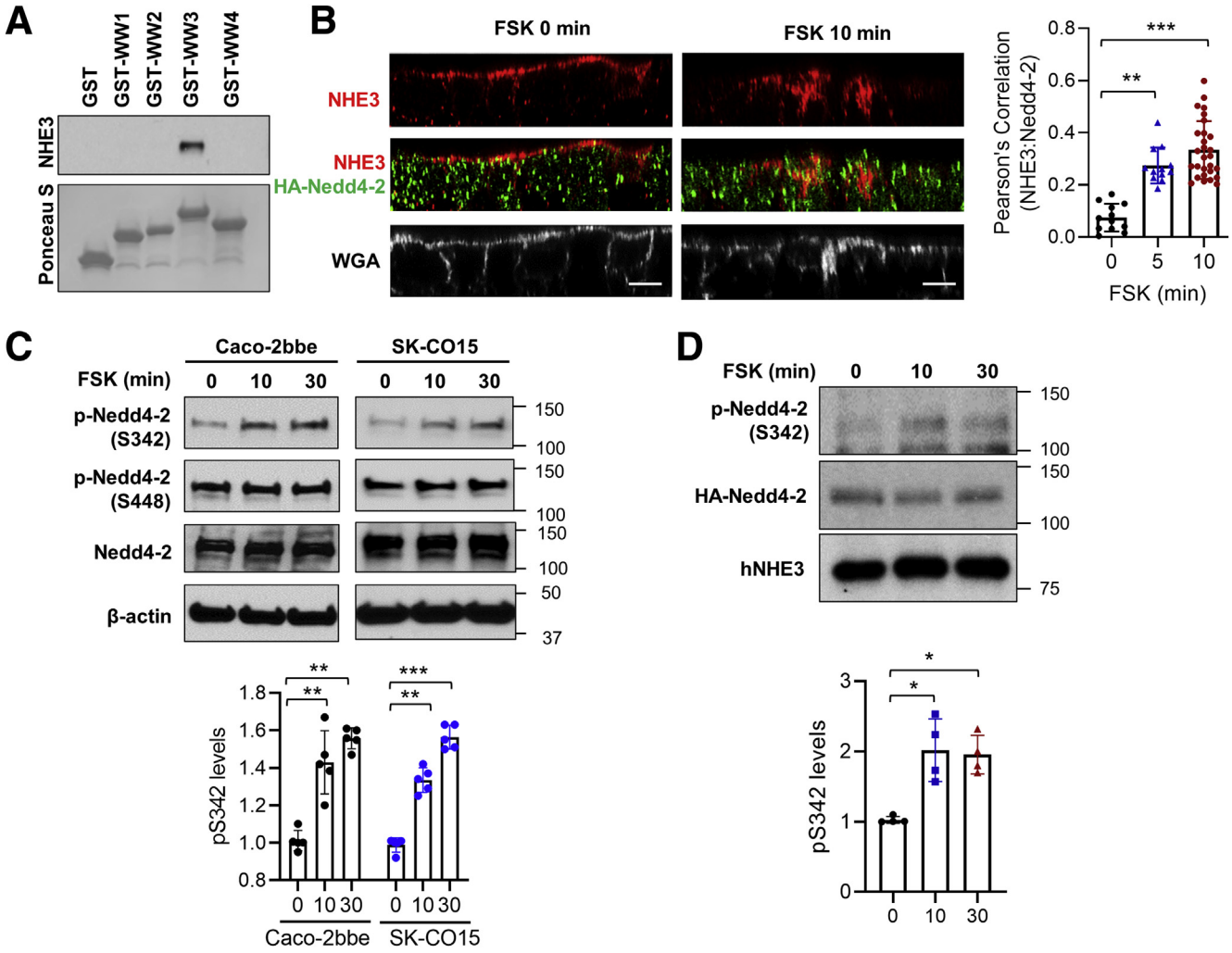

Figure 9. FSK increases the interaction of Nedd4-2 with hNHE3. (*A*) Binding of GST-tagged WW domains (WW1-4) of Nedd4-2 with hNHE3 was determined by pull-down assay. n = 3. (*B*) Subcellular localization of HA-Nedd4-2 and hNHE3 in Caco2bbe/hNHE3 cells after 5- or 10-minute FSK treatment was determined. Representative confocal cross-sectional views of hNHE3 (*red*), Nedd4-2 (*green*), and the apical membrane marker, wheat germ agglutinin (WGA; *white*), are shown. Scale bar: 10 μm. Results are representative of 3 independent experiments with triplicates of each experiment. Graph on the right represents Pearson's correlation coefficient of NHE3, and Nedd4-2 localization from more than 25 independent visual fields is shown. $^{**}P < .01$, $^{***}P < .001$ vs 0 minutes. (*C*) Caco-2bbe and SK-CO15 cells were treated with 10 μmol/L FSK for the indicated time, and phosphorylation of Nedd4-2 at Ser342 and S448 was determined using phosphorylation specific antibodies. Representative blots from 5 independent experiments are shown. $^{**}P < .01$, $^{***}P < .001$ vs 0 minutes. (*D*) Caco-2bbe/hNHE3 cells transfected with HA-Nedd4-2 were treated with FSK. hNHE3 was immunoprecipitated, and co-immunoprecipitated HA-Nedd4-2 was detected using anti-pS342 antibody and anti-HA antibody. Bottom panel shows immunoprecipitated hNHE3 identified using EM450 antibody. Representative results from 4 independent experiments are shown. $^{*}P < .05$ vs 0 minutes.

regulatory mechanism of hNHE3 that differs from that of non-human NHE3.

Discussion

The cause of diarrhea is multifactorial, but secretory diarrhea results often from bacterial and viral infections that cause excessive secretion and impaired absorption of electrolytes and fluid across the intestinal epithelium.[41] The current study was designed to determine whether the unique Nedd4-2–dependent regulation of hNHE3 contributes to diarrhea in humans that is perceived to be more severe and frequent compared with laboratory animals. We report the results comparing the regulation of NHE3s of human and non-human by adenylyl cyclase activators and EPEC. A major finding is that the presence of hNHE3 in the intestine exacerbates diarrhea caused by CTX and EPEC. This conclusion was inferred from increased water accumulation in hNHE3^{int} mouse intestine (a hallmark of diarrhea) compared with WT mouse intestine in response to CTX or EPEC.

Previously we reported that the basal internalization rate of hNHE3 in PS120 cells was almost twice the rate of rbNHE3 or ratNHE3.[17] We now found that FSK has

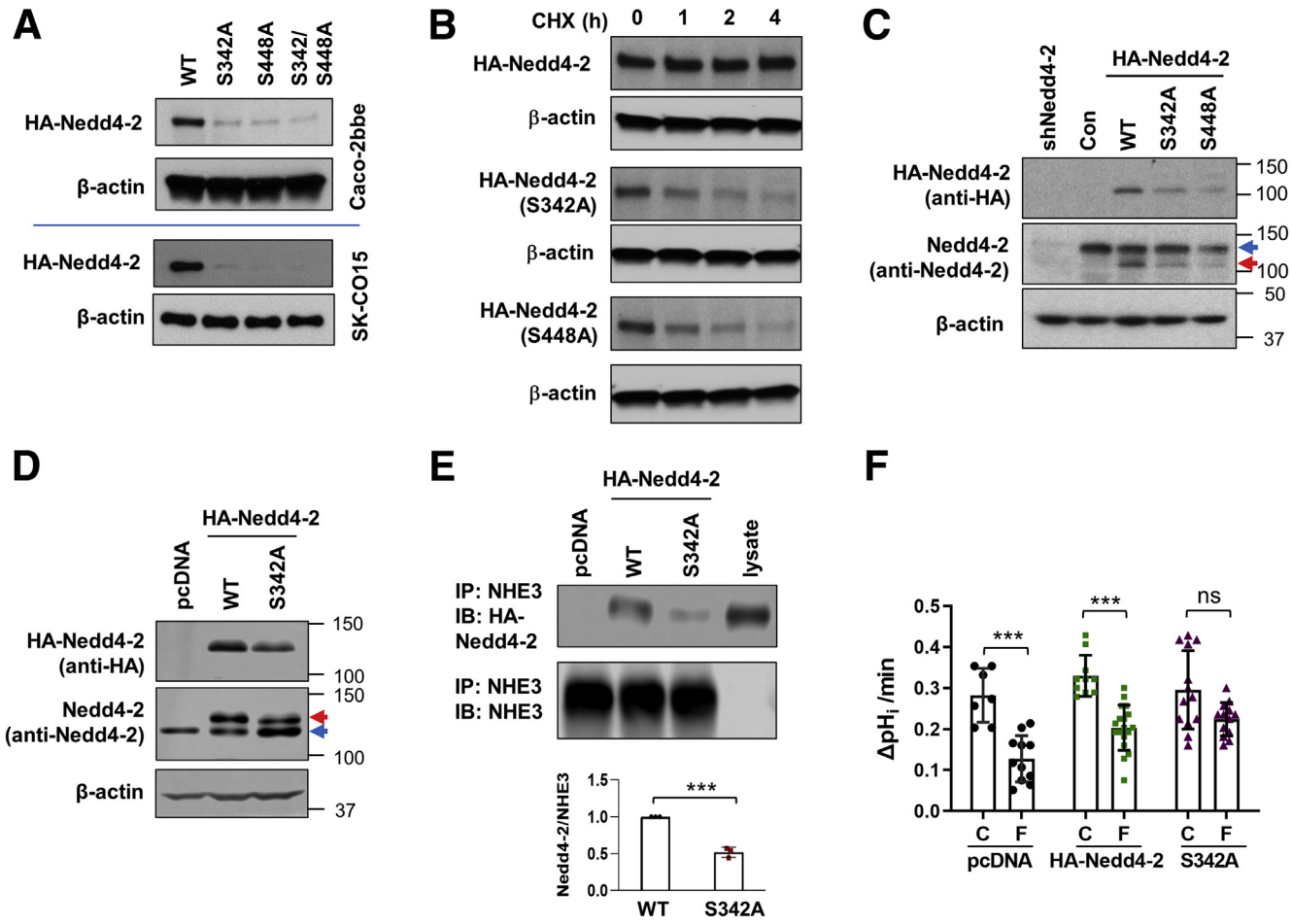

Figure 10. Phosphorylation of Nedd4-2 at S342 regulates its interaction with hNHE3 and FSK-mediated regulation of hNHE3. (*A*) Expression levels of HA-Nedd4-2 with S342A, S448A, or S342A/S448A mutation in Caco-2bbe (*upper*) and SK-CO15 (*lower*) cells were compared. Ha-Nedd4-2 variants were detected using mouse anti-HA antibody. n $\geq$ 5. (*B*) Caco-2bbe cells transfected with HA-Nedd4-2 variants were treated with CHX to block degradation, and HA-Nedd4-2 expression was determined. Representative blots from 3 independent experiments are shown. Caco-2bbe (*C*) and PS120 (*D*) cells were transiently transfected with HA-Nedd4-2 WT and mutants. *Top row*: immunoblots using anti-HA antibody depicting transfected HA-Nedd4-2. *Middle row*: immunoblots using anti-Nedd4-2 antibody. *Blue arrows*, endogenous Nedd4-2. *Red arrows*, HA-Nedd4-2. β-actin was used as a loading control. Results are representative of at least 3 independent experiments. (*E*) PS120 cells were transfected with HA-Nedd4-2 or S342A-HA-Nedd4-2 along with hNHE3. Interaction of Nedd4-2 with hNHE3 was assessed by co-immunoprecipitation. *Upper panel*, co-immunoprecipitated Nedd4-2. *Lower panel*, immunoprecipitated hNHE3. Representative results from 3 independent experiments are shown. Graph in the lower panel shows quantification of Nedd4-2 relative to hNHE3. ***$P < .001$. (*F*) Effect of FSK on NHE3 activity was determined in PS120 cells expressing WT and S342A Nedd4-2. Cells mock transfected with pcDNA were used as control. n = 7–17. **$P < .01$, ***$P < .001$.

heightened effects on hNHE3 than rbNHE3. There was a concentration-dependent inhibition of hNHE3 activity, reaching a greater level of inhibition of hNHE3 versus rbNHE3. This difference in hNHE3 activity was paralleled by increased fluid accumulation in the intestine of hNHE3^{int} mice after CTX administration. CTX causes an accumulation of intestinal fluid that contributes to diarrhea through activation of Cl^- secretion by CFTR and inhibition of Na^+ absorption by NHE3. The transgenic expression level of hNHE3 did not alter CFTR expression (mRNA) or activity, indicating that the difference in fluid absorption between hNHE3^{int} and WT mice was a result of the presence of hNHE3 in the intestine of hNHE3^{int} mice.

A growing body of evidence shows that imbalance of the gut microbiota increases the susceptibility to various pathogens, often resulting in diarrhea.[42] Reduced microbial diversity predisposes Nhe3$^{-/-}$ mice to colitis.[23,43] We found that transgenic hNHE3 expression largely reverses the dysbiosis caused by the absence of NHE3, although a more detailed microbial analysis is needed to compare the extent of the restoration.

The difference in intestinal fluid accumulation between hNHE3^{int} and WT mice was reproduced by EPEC, suggesting that the effects are not limited to PKA-mediated regulation. However, EPEC administration to hNHE3^{int} mice did not yield clear evidence for diarrhea, although increased stool water contents were observed intermittently. EPEC adhere

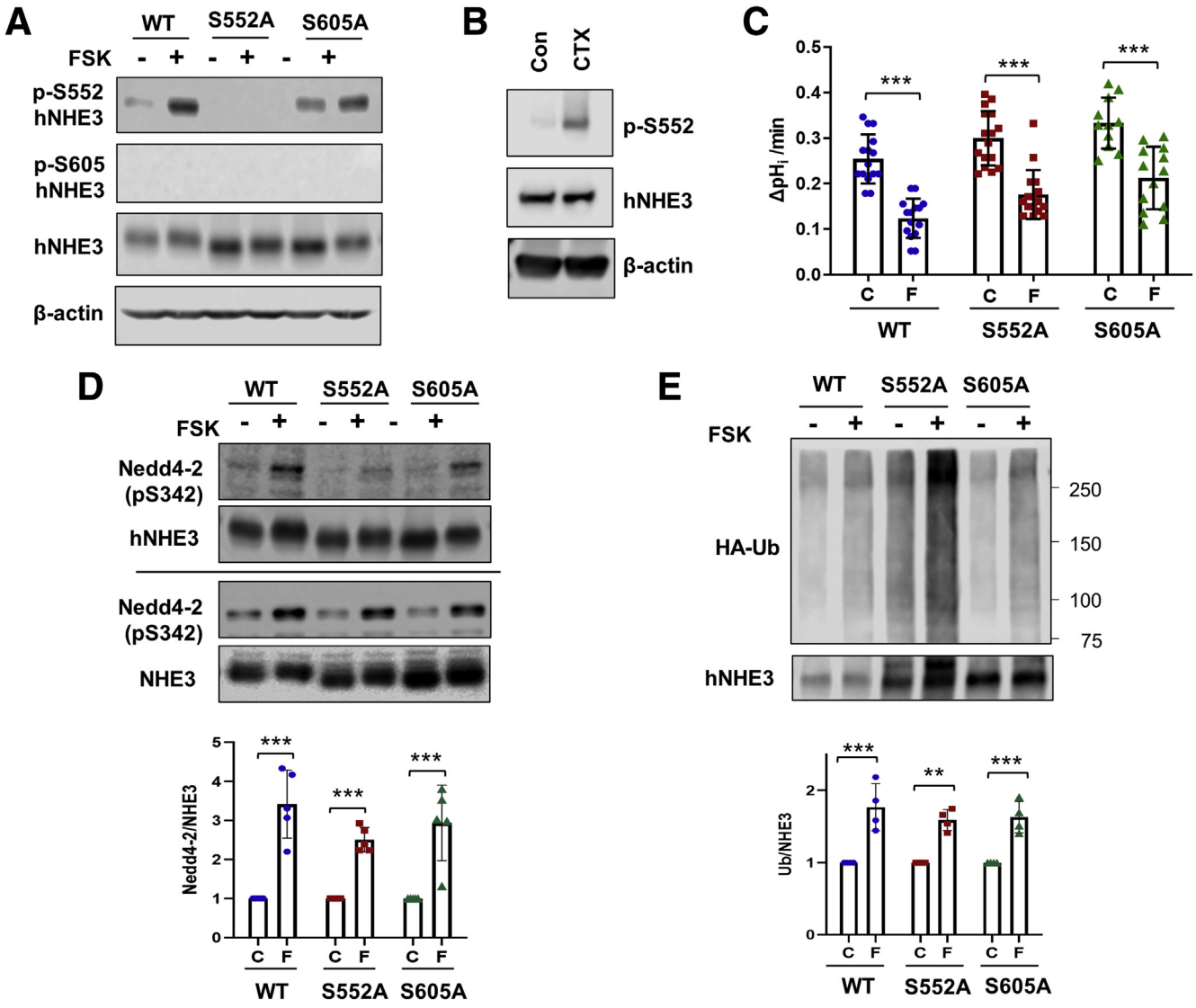

Figure 11. Inhibition of hNHE3 by FSK is independent of phosphorylation of hNHE3 at S552. (*A*) Caco-2bbe cells expressing hNHE3 with S552A or S605A mutation were treated with FSK for 10 minutes. Phosphorylation of hNHE3 at S552 and S605 was determined using anti-pS552 and anti-pS605 antibodies. n = 3. (*B*) Closed ileal loops were treated with CTX or dimethyl sulfoxide (*C*) for 30 minutes, and lysates were made from scraped intestinal epithelial layers. Phosphorylation at S552 and hNHE3 expression in the lysates were determined by Western blotting. n = 3. (*C*) NHE3 activities were determined in Caco-2bbe cells expressing hNHE3 variants that were treated with FSK (*F*) or dimethyl sulfoxide (*C*). n = 14–17. Results are presented as mean ± SD. ***$P < .001$ by multiple *t* test. (*D*) Caco-2bbe cells expressing hNHE3 variants were treated with FSK (*F*) or dimethyl sulfoxide (*C*) for 10 minutes. hNHE3 was immunoprecipitated (*second row*), and co-immunoprecipitated pS342-Nedd4-2 (*top row*) was determined. Bottom two lanes show immunoblots of pS342-Nedd4-2 and hNHE3 in cell lysates. Graph at the bottom shows quantification of p-Nedd4-2/hNHE3 ratios from 5 independent experiments. n = 5. ***$P < .001$. (*E*) Ubiquitination levels of hNHE3 variants were determined by immunoprecipitation of hNHE3, followed by immunoblotting with anti-Ub antibodies. Lower panel shows immunoprecipitated hNHE3. Ub levels normalized to hNHE3 immunoprecipitated are shown on the bottom. n = 4. **$P < .01$, ***$P < .001$ by multiple *t* test.

to the surface of enterocytes via an "attaching and effacing" mechanism, but the efficacy of EPEC colonization in small animals such as mouse and rat is contentious. EPEC colonization in the intestine of 6- to 8-week-old C57Bl/6 mice has been demonstrated.[34,44] On the other hand, no EPEC colonies were found in Swiss NIH mice, suggesting that EPEC colonization is influenced by the genetic background.[45] hNHE3^{int} mice are in the FVB/N genetic background, and inefficient EPEC colonization in these mice could have led to the lack of clear differences between hNHE3^{int} and WT mice.

Consistent with our previous study,[17] the regulation of hNHE3 by CTX and EPEC is Nedd4-2–dependent. Blockade of Nedd4-2 interaction by Nedd4-2 knockdown or mutations in the PY motif of hNHE3 ablated the effects of FSK and EPEC. In addition, CTX and EPEC increased ubiquitination levels of hNHE3. However, our current study investigating Nedd4-2 dependence was limited to in vitro assays because

our efforts to generate hNHE3^{int} mice in the absence of Nedd4-2 were not successful. The best characterized substrate of Nedd4-2 is the epithelial Na^+ channel (ENaC). Nedd4-2 deletion causes up-regulation of ENaC in the kidney and lung, causing electrolyte imbalance and respiratory stress.[46,47] ENaC in the colon plays an important role in preserving sodium ions. However, colon-specific deletion of ENaC in mice does not cause diarrhea, despite sodium loss and aldosterone resistance,[48] and it is not clear whether colonic ENaC function is altered in Nedd4-2 knockout mice. In comparison, intestine-specific deletion of NHE3 causes congenital sodium diarrhea in mice.[49] Therefore, whether Nedd4-2 deficiency alters NHE3-dependent sodium and fluid absorption in vivo awaits future investigations.

Nedd4-2 interacts with its substrates, including hNHE3 and ENaC, at cell surface.[17,50] IF microscopic analysis of hNHE3 and Nedd4-2 immediately after FSK treatment revealed significant overlaps of IF signals of hNHE3 and Nedd4-2, suggesting dynamic regulation of hNHE3–Nedd4-2 interaction at the apical region of the cells. Previous studies have shown phosphorylation of Nedd4-2 by PKA and serum and glucocorticoid regulated kinase 1 in COS-7 cells and *Xenopus* oocytes.[37,38] Consistently, FSK induced phosphorylation of Nedd4-2 at S342 in colonic epithelial cells, and we observed increased presence of p-S342–Nedd4-2 in the NHE3-containing immunocomplex. Using PS120 cells, we demonstrated that the S342A mutation impaired Nedd4-2 binding to hNHE3. However, the assessment of the interaction between the S342A mutant and hNHE3 in Caco-2 cells was hindered by the low expression levels of S342A (and S448). We found that phosphorylation of Nedd4-2 is important for the maintenance of Nedd4-2 expression in colonic epithelial cells. Phosphorylation-dependent Nedd4-2 stabilization has previously been observed. Dephosphorylation at S448 by a phosphatase reduced Nedd4-2 abundance, whereas phosphorylation of Xenopus Nedd4-2 at S444 (equivalent to S448 in human Nedd4-2) increased its expression.[51,52]

We demonstrated in this study that hNHE3 regulation by EPEC is PKC dependent. Previous studies have shown that EPEC rapidly activate host cell PKC and disrupt epithelial tight junctions through the activation of PKC-ζ, and acute activation of NHE2 by EPEC has been shown to be dependent on PKCα and PKCε.[30,53,54] Although whether EPEC-mediated NHE3 regulation is mediated by PKC has not been studied prior to the current study, there is an unmistakable similarity between the effects of PKC and EPEC on the different NHE isoforms. A study in PS120 cells has shown that the PKC activating phorbol 12-myristate 13-acetate inhibits NHE1 and NHE2 but activates NHE3.[55] Interestingly, Nedd4-2 is activated by PKC to promote ubiquitination of membrane proteins, including cation amino acid transporter CAT-1, glutamate transport GLT-1, and organic anion transporter 1.[56–58] Future studies are needed to investigate the mechanism of PKC-dependent regulation of Nedd4-2.

Activation of PKA by FSK, 8-bromo-cyclic adenosine monophosphate, parathyroid hormone, and dopamine results in phosphorylation of NHE3.[11,12,39,59] Phosphopeptide mapping of NHE3 with mutational alteration of several serines has identified S552 and S605 as the primary sites of PKA-dependent phosphorylation in rat NHE3.[11,39] Recently, NHE3 in human renal proximal tubule cells was shown to be phosphorylated at S552 by gastrin-mediated signaling, but interestingly this effect was PKC-dependent and independent of PKA.[60] We showed here that FSK increased phosphorylation at S552 of hNHE3 in Caco-2bbe cells and hNHE3^{int} mouse intestine. One significant finding from the current study is that S552A and S605A mutations did not block PKA-mediated inhibition of hNHE3. These results contradict the previous studies on rat NHE3 that phosphorylation at these sites is a prerequisite for NHE3 regulation by PKA.[11,39] In addition, the S552A and S605A mutants co-immunoprecipitated pS342–Nedd4-2, and the ubiquitination levels of S552A and S605A mutants were elevated in response to FSK, suggesting that phosphorylation of hNHE3 at these serines does not affect Nedd4-2–mediated ubiquitination of hNHE3. It is not clear how PKA is able to inhibit hNHE3 without altering hNHE3 phosphorylation. On the other hand, despite the importance of phosphorylation at S552 and S605 for the regulation of rat NHE3,[11,39] how the phosphorylation impacts NHE3 is not clear. Previous studies using opossum kidney cells and rat kidney have indicated that phosphorylation of NHE3 does not directly impact the antiporter activity.[61,62] These studies imply that NHE3 phosphorylation elicits endocytosis of NHE3. Although the mechanical link between NHE3 phosphorylation and endocytosis is not known, dynamin and clathrin are involved in this process.[12,59,63] Since the initial description of ubiquitination as a mechanism of protein degradation, it has emerged as a major player in endocytosis of membrane proteins.[64,65] Ubiquitinated cargoes can be internalized via clathrin-dependent as well as independent pathways.[66,67] In addition, different clathrin adaptors may be involved in Ub-dependent versus Ub-independent internalization of cargoes.[68,69] In the case of hNHE3, the internalization is not triggered by phosphorylation of hNHE3, but instead it is mediated by Nedd4-2–dependent ubiquitination. We postulate that inhibition of hNHE3 and non-human NHE3s is mediated via alternative mechanisms of clathrin-mediated endocytosis involving different adaptor proteins. In addition, we speculate that inhibition of hNHE3 is more efficient in part because Ub ligation occurs at multiple sites, enabling increased recruitment of clathrin-mediated endocytic machinery. Whether hNHE3 is regulated by other enteropathogenic bacteria via a similar mechanism remains to be determined.

The current study demonstrates that the effects of CTX and EPEC are greater in hNHE3^{int} mice compared with WT mice. However, we recognize a few potential limitations of the current hNHE3^{int} mouse model. First, because of the transgenic construct of hNHE3 gene, it is likely that more than 2 copies of hNHE3 gene are present, which result in higher basal expression levels and activity compared with WT mice. Second, hNHE3 is driven by the villin promoter so that any regulation at the transcription level is absent. This

limits the use of the model for a long-term study because *Nhe3* expression can be transcriptionally suppressed by proinflammatory cytokines.[70] Third, the villin promoter might have caused the expression of hNHE3 protein in lower crypt cells that are normally devoid of NHE3 expression.[71] This could have contributed to the elevated basal activity of NHE3, although we have not specifically investigated the status of hNHE3 expression or activity in the lower part of the crypts. These limitations can be overcome with a knock-in mouse model that replaces mouse NHE3 with hNHE3 under the control of the endogenous NHE3 promoter.

With these limitations, our data demonstrate that CTX and EPEC augment the inhibition of hNHE3 via ubiquitination of hNHE3 that is distinct from the regulation of non-human NHE3. Inhibition of hNHE3 is dependent on Nedd4-2, which ubiquitinates and facilitates internalization of hNHE3. This unique biochemical feature of hNHE3 potentiates Na^+ and water loss, and it may contribute to diarrheal symptoms occurring in humans.

Materials and Methods

Reagents and Antibodies

CTX and FSK were purchased from Sigma-Aldrich (St Louis, MO). EPEC (E2348/69) and commensal *E coli* EFC-1 and EPEC were from Jan Klapproth (University of Pennsylvania, Philadelphia, PA).[72,73] Rabbit polyclonal anti-NHE3 antibody EM450 and mouse monoclonal anti-VSVG P5D4 were previously described.[22,74] Commercial antibodies used are listed in Table 1. All other chemicals were obtained from Sigma-Aldrich or EMD Millipore (Billerica, MA), unless otherwise specified.

Cell Culture and Plasmids

Caco-2bbe and SK-CO15 cells were cultured as previously described.[22] pcDNA3.1 construct carrying hNHE3 (pcDNA-hNHE3V) or rbNHE3 (pcDNA-rbNHE3V) with a C-terminal VSVG epitope has been described.[17] Caco-2bbe cells expression hNHE3 previously generated were used otherwise specified.[26] Caco-2bbe cells were stably transfected with pcDNA-rbNHE3 and acid-selected as previously described.[17] The lentiviral plasmid pLKO.1 containing shNedd4-2 or a scrambled control shRNA (shCon) was purchased from Sigma-Aldrich. pCI-HA-NEDD4L with or without a mutation in S342 or S448 was acquired from Dr Massague/Addgene (plasmid #27016, 27036, and 27037). The coding cDNA was subcloned into pcDNA3.1/Hygro (Invitrogen, Carlsbad, CA). hNHE3 constructs with S552A and S605A mutation were generated using pCDNA/hNHE3V as a template by using a QuickChange site-directed mutagenesis kit (Stratagene, San Diego, CA). The oligonucleotide primers designed to introduce the mutations are as follows (codon changes are underlined): forward primer S552A, 5'-GCT GAG GGA GAG CGC GGG GCC CTG GCC TTC ATC CGC TCC-3'; reverse primer S552A, 5'-GGA GCG GAT GAA GGC CAG GGC CCC GCG CTC TCC CTC AGC-3'; forward primer S605A, 5'-TCT CTG GAG CAG CGA CGG GCC ATC CGG GAC GCG GAG GAC ATG-3'; reverse primer S605A, 5'-CAT GTC CTC CGC GTC CCG GAT GGC CCG TCG CTG CTC CAG AGA-3'. The presence of mutation was confirmed by nucleotide sequencing.

Bacterial Culture

EPEC and EFC-1 were grown overnight in LB broth. On the next day, 900 μL of overnight culture were transferred into 30 mL of antibiotics-free Dulbecco modified Eagle medium and grown to an OD_{600} of 0.4. Bacteria were pelleted and resuspended in 4 mL fresh medium. Caco-2bbe cells cultured to 10–14 days after confluence in 6-cm dishes were cultured overnight in the absence of penicillin/streptomycin. Caco-2 cells were then inoculated with 1×10^8 colony-forming unit of bacteria per well for up to 90 minutes. For in vivo perfusion assays, 1 mL of *E coli* was added to 10 mL perfusion buffer.

Generation of hNHE3^{int} Mice

The hNHE3 cDNA with a carboxyl-terminal VSVG tag was amplified by polymerase chain reaction (PCR) using the primer pair: 5'-AGCGTACGCCACCATGTGGGGACT CGGGGCCCG -3' (forward) and 5'-GGACGCGTTTACTTGCC-CAGCCGGTTCATC -3' (reverse). The PCR product was cloned into the pBS-KS/Villin MES vector using BsiWI and MluI sites.[71] The sequence of hNHE3 in pBS-KS was verified by sequencing. The transgene was excised with SalI, purified, and injected into the pronuclei of fertilized eggs of

Table 1. Antibodies Used in the Study

Name of antigen	Catalog number	Vendor
Ubiquitin	sc-8017 (P5D1)	Santa Cruz Biotechnology
NHE3	NHE31-A	Alpha Diagnostics
NEDD4L	46521	Abcam
Phospho-NEDD4L (S342)	12146	Cell Signaling Technology
Phospho-NEDD4L (S448)	8063	Cell Signaling Technology
HA	C29F4	Cell Signaling Technology
β-actin	4967	Cell Signaling Technology
Anti-phospho-NHE3 (S552)	#MABN2415 (clone 14D5)	Millipore
Anti-phospho-NHE3 (S605)	#MABN2414 (clone 10A8)	Millipore

FVB/N mice at the Mouse Transgenic and Gene Targeting Core at Emory University (Atlanta, GA). The hNHE3 transgene was identified by PCR analysis of tail genomic DNA using the following primers: 5'-AGCAGTACCTGTACAAGCCG-3' (forward) and 5'-CTCCATGGGCAGCTTCCCATTGG-3' (reverse) for hNHE3 transgene. Murine NHE3 genotyping was determined by using primers previously described.[4] Transgenic expression of hNHE3 in the intestine was confirmed by Western blotting using anti-VSVG antibody. *Slc9a*-deficient (*Nhe3*$^{-/-}$) mice on the mixed 129/Black Swiss genetic background were previously described.[4] *Nhe3*$^{-/-}$ mice regenerated on the FBV/N were obtained from Drs Ghishan and Kiera at the University of Arizona (Tucson, AZ). Two hNHE3 transgenic male mice expressing both human *Slc9a* transgene and endogenous mouse *Slc9a* gene were mated with female *Nhe3*$^{-/-}$ mice to obtain offspring expressing one allele of mouse *Slc9a* gene and transgenic human *Slc9a* gene. Resulting male mice from the initial breeding were crossed with female *Nhe3*$^{-/-}$ mice to generate mice that express human Slc9a transgene without mouse Slc9a gene. These mice were labeled hNHE3^{int} mice. Because the initial estimation of hNHE3 expression in the intestinal epithelium by Western blotting was high, hNHE3^{int} male mice were backcrossed with female *Nhe3*$^{-/-}$ mice for 3 generations to reduce the expression levels of transgenic hNHE3. All animal experiments were conducted under approval by the Institutional Animal Care and Use Committee of Emory University and in accordance with the NIH Guide for the Care and Use of Laboratory Animals.

Co-Immunoprecipitation and Western Blot

Co-immunoprecipitation experiments were performed using lysates from Caco-2bbe cells or mouse intestinal mucosa prepared using lysis buffer (Cell Signaling, Danvers, MA) containing 150 mmol/L NaCl, 1 mmol/L β-glycerophosphate, 2.5 mmol/L sodium pyrophosphate, 1 mmol/L Na_2 EDTA, 1 mmol/L EGTA, 1 mmol/L Na_3VO_4, 1 μg/mL leupeptin, 1% Triton X-100, and protease inhibitors cocktail tablets (Roche, Indianapolis, IN). Lysate (500 μg) was precleared by incubation with 30 μL of protein A-Sepharose beads for 1 hour, and the supernatant was then incubated overnight with a primary antibody (anti-HA, anti-VSVG, or anti-NHE3 antibody). Immunocomplex was purified by incubating with 50 μL of protein A-Sepharose beads for 1 hour, followed by 3 washes in lysis buffer and 2 washes in phosphate-buffered saline. All of the above steps were performed at 4°C or on ice. Beads eluted with 2.5× Laemmli buffer. Cell lysates and eluted samples were separated by sodium dodecyl sulfate-polyacrylamide gel electrophoresis. Western immunoblotting and quantification were performed as described previously.[17,25]

Histologic and IF Analysis

Ileal and colonic sections from WT, hNHE3^{int}, and NHE3$^{-/-}$ mice were harvested, rinsed in Hank's buffered saline solution (HBSS), opened lengthwise, and fixed in 10% neutral buffered formalin (Electron Microscopy Sciences, Hatfield, PA). Fixed tissues were embedded in paraffin, and 5-μm-thick sections were stained with hematoxylin-eosin for light microscopic examination. IF staining of hNHE3 and mouse NHE3 with anti-NHE3 antibody (Alpha Diagnostics, Burlington, NC) was performed as previously described.[75]

Quantitative Real-Time PCR

Total RNA was extracted from intestinal mucosal scrapes or cultured cells using the RNeasy Mini kit (Qiagen, Hilden, Germany). One μg of total RNA was used for cDNA synthesis using a First Strand cDNA Synthesis Kit (Thermo Fisher Scientific, Waltham, MA) according to the manufacturer's instruction. Quantitative PCR was performed with iQ SYBR Green Supermix (Bio-Rad Laboratories, Hercules, CA) on a Mastercycler Realplex (Eppendorf, Hamburg, Germany). PCR primer sequences are listed in Table 2.

Table 2. Primer Sequences for Real-Time PCR Analysis

Target	Forward primer	Reverse primer
CFTR[a]	AGAGCAGTTTCCTGGACAGC	CCAGCGAAGGCTTGTTTTAG
DRA[a]	AATGCTGATGCAGTTTGCTG	TGCTCCTTCCAACATTAGCC
NHE2[a]	ACTGGGGTCACAACTTCTGG	CTTCACGGCAGTCATTGAGA
β-actin[a]	TACAGCTTCACCACCACAGC	AAGGAAGGCTGGAAAAGAGC
Universal[b]	AAACTCAAA(G/T)GAATTGACGG	CTCAC(G/A)(G/A)CACGAGCTGAC
Bacteroidetes[b]	C(G/A)AACAGGATTAGATACCCT	GGTAAGGTTCTTCGCGTAT
Firmicutes[b]	TGAAACT(T/C)AAAGGAATTGACG	ACCATGCACCACCTGTC
Actinobacteria[b]	TACGGCCGCAAGGCTA	TC(G/A)TCCCCACCTTCCTCCG
α-Proteobacteria[b]	C(A/C/T)AGTGTAGAGGTGAAATT	CCCCGTCAATTCCTTTGAGTT
γ-Proteobacteria[b]	TCGTCAGCTCGTGT(T/C)GTGA	TCGTCAGCTCGTGTCGTGA
Clostridium leptum (IV) [b]	CCTTCCGTGCCG(G/C) AGTTA	GAATTAAACCACATACTCCACTGCTT
Clostridium coccoides[b]	AAATGACGGTACCTGACTAA	CTTTGAGTTTCATTCTTGCGAA

Primer sequences were adapted from [a]reference 25 and [b]reference 23.

Microbiota Analysis

Mice were anesthetized with isoflurane and euthanized by cervical dislocation. The intestine was removed under sterile conditions, and the contents of the cecum were collected, snap frozen in liquid nitrogen, and stored at −80°C until needed. Bacterial total DNA (genomic DNA) was isolated using the QIAamp DNA Stool Mini Kit (Qiagen, Frederick, MD). Specific primer sets were used in the amplification of microbial 16S rRNA gene on a Real Plex4 RealTime System (Eppendof, Hauppauge, NY) as previously published.[23] The sequences of primers are listed in Table 2.

Fluid Accumulation in Ileal Closed Loop

Mice were anesthetized using a ketamine/xylazine cocktail (100 mg/kg ketamine and 10 mg/kg xylazine), and a small incision was made in the abdomen. Two sections of ileum approximately 3.5–6 cm were tied off using surgical string. One loop was injected with 100 μL of HBSS control buffer, and the second loop was injected with 10 μg CTX (diluted in 100 μL HBSS). To inhibit NHE3 activity, NHE3 inhibitor S3226 (0.5 mg in 100 μL HBSS) was added to each isolated intestinal loop. The incision in the abdominal cavity was sutured, and mice were allowed to recover for 5 hours after injection. Mice were euthanized using isoflurane and cervical dislocation. Loops were excised, photographed, measured for length, and weighed. The weight to length ratio was calculated and used as a measure of fluid accumulation over the 5-hour treatment period.

Intestinal Water Flux Measurement

Intestinal water flux was measured as previously reported.[26] Briefly, a mouse anesthetized with sodium pentobarbital was placed on a 37°C heating block, and a small incision was made in the abdomen. An approximately 5-cm loop of the ileum (between 5 and 10 cm upstream of cecum) cannulated at the proximal and distal ends was flushed with saline for 10 minutes. This was followed by perfusion of pre-warmed perfusion solution (mmol/L: 118.4 NaCl, 4.7 KCl, 2.52 $CaCl_2$, 1.18 $MgSO_4$, 25 Na gluconate, 1.18 KH_2PO_4, pH 7.4) at 1 mL/min for 2 hours. When needed, EPEC or control EFC-1 bacteria (multiplicity of infection: 200) were added to the perfusion buffer. CFinh-172 (250 μg/kg) was administered by intraperitoneal injection to each mouse 1 hour before the start of perfusion. CTX (0.5 μg/mL) was added to the perfusate. Intestinal water flux was recorded by calculating a change in the volume of perfusion buffer in a reservoir every 10 minutes over the course of a 90- to 120-minute perfusion period.

Na^+ Dependent Intracellular pH Recovery

The Na^+-dependent changes in pH_i by NHE3 were determined using the ratio fluorometric, pH-sensitive dye 2',7'-bis-(2-carboxyethyl)-5-carboxyfluorescein acetoxymethyl ester as previously described.[22] Caco-2bbe cells grown for 10–14 days after confluence were treated with 10 μmol/L FSK for 30 minutes during dye loading. For experiments using EPEC, cells were infected at a multiplicity of infection of 20 for 90 minutes. For the measurement of NHE3 activity in mouse intestine, isolation of villi from mice ileum was performed as previously described.[75] In brief, mice were euthanized with isoflurane, and the ileum was flushed with cold phosphate-buffered saline to remove food particles. An equivalent segment of the proximal ileum (approximately 10 cm upstream of the cecum) was opened longitudinally and stabilized on a cooled stage. The villi were dissected under stereomicroscope using sharpened microdissection scissors. Isolated villi were mounted on coverslips and covered with light and solution penetrable polycarbonate membrane (GE, Minnetonka, MN). Coverslips were mounted on a perfusion chamber, placed on an inverted microscope, superfused with NH_4^+ buffer, followed by sequential perfusion with tetramethylammonium (130 mmol/L TMA-Cl, 20 mmol/L HEPES, 5 mmol/L KCl, 1 mmol/L TMA-PO_4, 2 mmol/L $CaCl_2$, 1 mmol/L $MgSO_4$, and 25 mmol/L glucose) and Na^+ buffer that drives Na^+-dependent pH recovery. Na^+ buffer was supplemented with 30 μmol/L HOE694 or 2 μmol/L dimethyl amiloride to inhibit NHE1 and NHE2 activities. The microfluorometry was performed using the Metafluor software (Molecular Devices, Sunnyvale, CA), and 2–3 traces of Na^+-dependent pH recovery were captured from each coverslip, each trace originating from an independent group of cells. For each experiment, a minimum of 4 coverslips per group were studied. Na^+/H^+ exchange rate was described by the initial rate of pH_i recovery, which was calculated by determining slopes along the pH_i recovery by linear least-squares analysis over a minimum of 7 seconds.

Detection of NHE3 Ubiquitination

Cells were lysed in cold lysis buffer supplemented with 10 μmol/L MG132 to inhibit proteasomal degradation. Equal amounts of cell lysates (typically 0.5 mg) were incubated overnight with EM450 antibody, followed by incubation with protein A-Sepharose beads for 1 hour. Immunocomplex was washed twice in lysis buffer and once in phosphate-buffered saline. NHE3 was eluted, resolved by sodium dodecyl sulfate-polyacrylamide gel electrophoresis, and immunoblotted with P4D1 antibody.

Surface Biotinylation

Surface biotinylation of NHE3 was performed as previously described.[25] Briefly, cells grown in Transwells 2 weeks after confluence were treated with or without FSK for the indicated times, followed by rinsing with cold phosphate-buffered saline. Then 0.5 mg/mL NHS-SS-biotin in borate buffer was added to the apical chamber for 10 minutes, rinsed, and lysed. An aliquot was retained as the total fraction representing the total cellular NHE3. One mg of lysate was incubated with streptavidin-agarose beads (Thermo Fisher Scientific), and biotinylated surface proteins were then eluted representing surface NHE3. Densitometric analysis was performed using Scion Image software (National Institutes of Health, Bethesda, MD).

Statistical Analysis

Statistical analysis was performed using independent samples two-tailed unpaired Student t test or analysis of variance (ANOVA), followed by the Tukey post hoc analysis. Results are presented as mean ± standard deviation (SD). Statistical analysis was performed using GraphPad Prism software (La Jolla, CA). A value of $P < .05$ was considered significant.

References

1. Cheng AC, McDonald JR, Thielman NM. Infectious diarrhea in developed and developing countries. J Clin Gastroenterol 2005;39:757–773.
2. Viswanathan VK, Hodges K, Hecht G. Enteric infection meets intestinal function: how bacterial pathogens cause diarrhoea. Nat Rev Microbiol 2009;7:110–119.
3. Zachos NC, Tse M, Donowitz M. Molecular physiology of intestinal Na+/H+ exchanger. Annu Rev Physiol 2005; 67:411–443.
4. Schultheis PJ, Clarke LL, Meneton P, Miller ML, Soleimani M, Gawenis LR, Riddle TM, Duffy JJ, Doetschman T, Wang T, Giebisch G, Aronson PS, Lorenz JN, Shull GE. Renal and intestinal absorptive defects in mice lacking the NHE3 Na+/H+ exchanger. Nat Genet 1998;19:282–285.
5. Janecke AR, Heinz-Erian P, Yin J, Petersen BS, Franke A, Lechner S, Fuchs I, Melancon S, Uhlig HH, Travis S, Marinier E, Perisic V, Ristic N, Gerner P, Booth IW, Wedenoja S, Baumgartner N, Vodopiutz J, Frechette-Duval MC, De Lafollie J, Persad R, Warner N, Tse CM, Sud K, Zachos NC, Sarker R, Zhu X, Muise AM, Zimmer KP, Witt H, Zoller H, Donowitz M, Muller T. Reduced sodium/proton exchanger NHE3 activity causes congenital sodium diarrhea. Hum Mol Genet 2015; 24:6614–6623.
6. Seidler U, Lenzen H, Cinar A, Tessema T, Bleich A, Riederer B. Molecular mechanisms of disturbed electrolyte transport in intestinal inflammation. Ann N Y Acad Sci 2006;1072:262–275.
7. Anderson CA, Boucher G, Lees CW, Franke A, D'Amato M, Taylor KD, Lee JC, Goyette P, Imielinski M, Latiano A, Lagace C, Scott R, Amininejad L, Bumpstead S, Baidoo L, Baldassano RN, Barclay M, Bayless TM, Brand S, Buning C, Colombel JF, Denson LA, De Vos M, Dubinsky M, Edwards C, Ellinghaus D, Fehrmann RS, Floyd JA, Florin T, Franchimont D, Franke L, Georges M, Glas J, Glazer NL, Guthery SL, Haritunians T, Hayward NK, Hugot JP, Jobin G, Laukens D, Lawrance I, Lemann M, Levine A, Libioulle C, Louis E, McGovern DP, Milla M, Montgomery GW, Morley KI, Mowat C, Ng A, Newman W, Ophoff RA, Papi L, Palmieri O, Peyrin-Biroulet L, Panes J, Phillips A, Prescott NJ, Proctor DD, Roberts R, Russell R, Rutgeerts P, Sanderson J, Sans M, Schumm P, Seibold F, Sharma Y, Simms LA, Seielstad M, Steinhart AH, Targan SR, van den Berg LH, Vatn M, Verspaget H, Walters T, Wijmenga C, Wilson DC, Westra HJ, Xavier RJ, Zhao ZZ, Ponsioen CY, Andersen V, Torkvist L, Gazouli M, Anagnou NP, Karlsen TH, Kupcinskas L, Sventoraityte J, Mansfield JC, Kugathasan S, Silverberg MS, Halfvarson J, Rotter JI, Mathew CG, Griffiths AM, Gearry R, Ahmad T, Brant SR, Chamaillard M, Satsangi J, Cho JH, Schreiber S, Daly MJ, Barrett JC, Parkes M, Annese V, Hakonarson H, Radford-Smith G, Duerr RH, Vermeire S, Weersma RK, Rioux JD. Meta-analysis identifies 29 additional ulcerative colitis risk loci, increasing the number of confirmed associations to 47. Nat Genet 2011;43:246–252.
8. Zhu XC, Sarker R, Horton JR, Chakraborty M, Chen TE, Tse CM, Cha B, Donowitz M. Nonsynonymous single nucleotide polymorphisms of NHE3 differentially decrease NHE3 transporter activity. Am J Physiol Cell Physiol 2015;308:C758–C766.
9. Das S, Jayaratne R, Barrett KE. The role of ion transporters in the pathophysiology of infectious diarrhea. Cell Mol Gastroenterol Hepatol 2018;6:33–45.
10. Field M. Intestinal ion transport and the pathophysiology of diarrhea. J Clin Invest 2003;111:931–943.
11. Zhao H, Wiederkehr MR, Fan L, Collazo RL, Crowder LA, Moe OW. Acute inhibition of Na/H exchanger NHE-3 by cAMP: role of protein kinase a and NHE-3 phosphoserines 552 and 605. J Biol Chem 1999; 274:3978–3987.
12. Hu MC, Fan L, Crowder LA, Karin-Jimenez Z, Murer H, Moe OW. Dopamine acutely stimulates Na/H exchanger (NHE3) endocytosis via clathrin-coated vesicles: dependence on protein kinase A-mediated NHE3 phosphorylation. J Biol Chem 2001;276:26906–26915.
13. Singh V, Yang J, Yin J, Cole R, Tse M, Berman DE, Small SA, Petsko G, Donowitz M. Cholera toxin inhibits SNX27-retromer-mediated delivery of cargo proteins to the plasma membrane. J Cell Sci 2018;131:jcs218610.
14. Chen HD, Frankel G. Enteropathogenic Escherichia coli: unravelling pathogenesis. FEMS Microbiol Rev 2005; 29:83–98.
15. Hodges K, Alto NM, Ramaswamy K, Dudeja PK, Hecht G. The enteropathogenic Escherichia coli effector protein EspF decreases sodium hydrogen exchanger 3 activity. Cell Microbiol 2008;10:1735–1745.
16. Piper RC, Lehner PJ. Endosomal transport via ubiquitination. Trends Cell Biol 2011;21:647–655.
17. No YR, He P, Yoo BK, Yun CC. Unique regulation of human Na+/H+ exchanger 3 (NHE3) by Nedd4-2 ligase that differs from non-primate NHE3s. J Biol Chem 2014; 289:18360–18372.
18. Yang B, Kumar S. Nedd4 and Nedd4-2: closely related ubiquitin-protein ligases with distinct physiological functions. Cell Death Differ 2010;17:68–77.
19. Armando I, Villar VA, Jones JE, Lee H, Wang X, Asico LD, Yu P, Yang J, Escano CS Jr, Pascua-Crusan AM, Felder RA, Jose PA. Dopamine D3 receptor inhibits the ubiquitin-specific peptidase 48 to promote NHE3 degradation. FASEB J 2014;28:1422–1434.
20. Han Y, Yun CC. Ubiquitin-specific peptidase 7 (USP7) and USP10 mediate deubiquitination of human NHE3 regulating its expression and activity. FASEB J 2020; 34:16476–16488.
21. Walsh NC, Kenney LL, Jangalwe S, Aryee KE, Greiner DL, Brehm MA, Shultz LD. Humanized mouse

models of clinical disease. Annual Review of Pathology 2017;12:187–215.
22. Yoo BK, Yanda MK, No YR, Yun CC. Human intestinal epithelial cell line SK-CO15 is a new model system to study Na(+)/H(+) exchanger 3. Am J Physiol Gastrointest Liver Physiol 2012;303:G180–G188.
23. Larmonier CB, Laubitz D, Hill FM, Shehab KW, Lipinski L, Midura-Kiela MT, McFadden RM, Ramalingam R, Hassan KA, Golebiewski M, Besselsen DG, Ghishan FK, Kiela PR. Reduced colonic microbial diversity is associated with colitis in NHE3-deficient mice. Am J Physiol Gastrointest Liver Physiol 2013;305:G667–G677.
24. Zhou Q, Clarke L, Nie R, Carnes K, Lai LW, Lien YH, Verkman A, Lubahn D, Fisher JS, Katzenellenbogen BS, Hess RA. Estrogen action and male fertility: roles of the sodium/hydrogen exchanger-3 and fluid reabsorption in reproductive tract function. Proc Natl Acad Sci U S A 2001;98:14132–14137.
25. He P, Zhao L, Zhu L, Weinman EJ, De Giorgio R, Koval M, Srinivasan S, Yun CC. Restoration of Na+/H+ exchanger NHE3-containing macrocomplexes ameliorates diabetes-associated fluid loss. J Clin Invest 2015; 125:3519–3531.
26. Lin S, Yeruva S, He P, Singh AK, Zhang H, Chen M, Lamprecht G, de Jonge HR, Tse M, Donowitz M, Hogema BM, Chun J, Seidler U, Yun CC. Lysophosphatidic acid stimulates the intestinal brush border Na+/H+ exchanger 3 and fluid absorption via LPA5 and NHERF2. Gastroenterology 2010;138:649–658.
27. Ma TH, Thiagarajah JR, Yang H, Sonawane ND, Folli C, Galietta LJV, Verkman AS. Thiazolidinone CFTR inhibitor identified by high-throughput screening blocks cholera toxin-induced intestinal fluid secretion. J Clin Invest 2002;110:1651–1658.
28. Thiagarajah JR, Broadbent T, Hsieh E, Verkman AS. Prevention of toxin-induced intestinal ion and fluid secretion by a small-molecule CFTR inhibitor. Gastroenterology 2004;126:511–519.
29. Sasaki M, Sitaraman SV, Babbin BA, Gerner-Smidt P, Ribot EM, Garrett N, Alpern JA, Akyildiz A, Theiss AL, Nusrat A, Klapproth J-MA. Invasive Escherichia coli are a feature of Crohn's disease. Lab Invest 2007; 87:1042–1054.
30. Tomson FL, Koutsouris A, Viswanathan VK, Turner JR, Savkovic SD, Hecht G. Differing roles of protein kinase C-zeta in disruption of tight junction barrier by enteropathogenic and enterohemorrhagic Escherichia coli. Gastroenterology 2004;127:859–869.
31. Ghanekar Y, Chandrashaker A, Visweswariah SS. Cellular refractoriness to the heat-stable enterotoxin peptide is associated with alterations in levels of the differentially glycosylated forms of guanylyl cyclase C. Eur J Biochem 2003;270:3848–3857.
32. Bijvelds MJC, Tresadern G, Hellemans A, Smans K, Nieuwenhuijze NDA, Meijsen KF, Bongartz JP, Ver Donck L, de Jonge HR, Schuurkes JAJ, De Maeyer JH. Selective inhibition of intestinal guanosine 3,5-cyclic monophosphate signaling by small-molecule protein kinase inhibitors. J Biol Chem 2018;293:8173–8181.
33. Hurley BP, McCormick BA. Translating tissue culture results into animal models: the case of Salmonella typhimurium. Trends Microbiol 2003;11:562–569.
34. Savkovic SD, Villanueva J, Turner JR, Matkowskyj KA, Hecht G. Mouse model of enteropathogenic Escherichia coli infection. Infect Immun 2005;73:1161–1170.
35. Hecht G, Koutsouris A. Enteropathogenic E coli attenuates secretagogue-induced net intestinal ion transport but not Cl- secretion. Am J Physiol 1999; 276:G781–G788.
36. Staub O, Rotin D. Role of ubiquitylation in cellular membrane transport. Physiol Rev 2006;86:669–707.
37. Debonneville C, Flores SY, Kamynina E, Plant PJ, Tauxe C, Thomas MA, Munster C, Chraibi A, Pratt JH, Horisberger JD, Pearce D, Loffing J, Staub O. Phosphorylation of Nedd4-2 by Sgk1 regulates epithelial Na(+) channel cell surface expression. EMBO J 2001; 20:7052–7059.
38. Snyder PM, Olson DR, Kabra R, Zhou R, Steines JC. cAMP and serum and glucocorticoid-inducible kinase (SGK) regulate the epithelial Na+ channel through convergent phosphorylation of Nedd4-2. J Biol Chem 2004;279:45753–45758.
39. Kurashima K, Yu FH, Cabado AG, Szabo EZ, Grinstein S, Orlowski J. Identification of sites required for down-regulation of Na/H exchanger NHE3 activity by cAMP-dependent protein kinase. J Biol Chem 1997; 272:28672–28679.
40. Kocinsky HS, Girardi ACC, Biemesderfer D, Nguyen T, Mentone S, Orlowski J, Aronson PS. Use of phospho-specific antibodies to determine the phosphorylation of endogenous Na+/H+ exchanger NHE3 at PKA consensus sites. Am J Physiol Renal Physiol 2005; 289:F249–F258.
41. Thiagarajah JR, Donowitz M, Verkman AS. Secretory diarrhoea: mechanisms and emerging therapies. Nat Rev Gastroenterol Hepatol 2015;12:446–457.
42. Li Y, Xia S, Jiang X, Feng C, Gong S, Ma J, Fang Z, Yin J, Yin Y. Gut microbiota and diarrhea: an updated review. Frontiers in Cellular and Infection Microbiology 2021:11.
43. Kiela PR, Laubitz D, Larmonier CB, Midura-Kiela MT, Lipko MA, Janikashvili N, Bai A, Thurston R, Ghishan FK. Changes in mucosal homeostasis predispose NHE3 knockout mice to increased susceptibility to DSS-induced epithelial injury. Gastroenterology 2009; 137:965–975, 975 e961–e910.
44. Dupont A, Sommer F, Zhang K, Repnik U, Basic M, Bleich A, Kuhnel M, Backhed F, Litvak Y, Fulde M, Rosenshine I, Hornef MW. Age-dependent susceptibility to enteropathogenic Escherichia coli (EPEC) infection in mice. PLoS Pathog 2016;12:e1005616.
45. Frankel G, Phillips AD, Novakova M, Field H, Candy DC, Schauer DB, Douce G, Dougan G. Intimin from enteropathogenic Escherichia coli restores murine virulence to a Citrobacter rodentium eaeA mutant: induction of an immunoglobulin A response to intimin and EspB. Infect Immun 1996;64:5315–5325.
46. Shi PP, Cao XR, Sweezer EM, Kinney TS, Williams NR, Husted RF, Nair R, Weiss RM, Williamson RA, Sigmund CD, Snyder PM, Staub O, Stokes JB, Yang B.

Salt-sensitive hypertension and cardiac hypertrophy in mice deficient in the ubiquitin ligase Nedd4-2. Am J Physiol Renal Physiol 2008;295:F462–F470.
47. Boase NA, Rychkov GY, Townley SL, Dinudom A, Candi E, Voss AK, Tsoutsman T, Semsarian C, Melino G, Koentgen F, Cook DI, Kumar S. Respiratory distress and perinatal lethality in Nedd4-2-deficient mice. Nat Commun 2011;2:287.
48. Malsure S, Wang Q, Charles RP, Sergi C, Perrier R, Christensen BM, Maillard M, Rossier BC, Hummler E. Colon-specific deletion of epithelial sodium channel causes sodium loss and aldosterone resistance. J Am Soc Nephrol 2014;25:1453–1464.
49. Xue J, Thomas L, Tahmasbi M, Valdez A, Dominguez Rieg JA, Fenton RA, Rieg T. An inducible intestinal epithelial cell-specific NHE3 knockout mouse model mimicking congenital sodium diarrhea. Clin Sci (Lond) 2020;134:941–953.
50. Zhou R, Patel SV, Snyder PM. Nedd4-2 catalyzes ubiquitination and degradation of cell surface ENaC. J Biol Chem 2007;282:20207–20212.
51. Ho PY, Li H, Pavlov TS, Tuerk RD, Tabares D, Brunisholz R, Neumann D, Staruschenko A, Hallows KR. beta1Pix exchange factor stabilizes the ubiquitin ligase Nedd4-2 and plays a critical role in ENaC regulation by AMPK in kidney epithelial cells. J Biol Chem 2018; 293:11612–11624.
52. Ismail NA, Baines DL, Wilson SM. The phosphorylation of endogenous Nedd4-2 in Na(+)-absorbing human airway epithelial cells. Eur J Pharmacol 2014;732:32–42.
53. Crane JK, Oh JS. Activation of host cell protein kinase C by enteropathogenic Escherichia coli. Infect Immun 1997;65:3277–3285.
54. Hodges K, Gill R, Ramaswamy K, Dudeja PK, Hecht G. Rapid activation of Na+/H+ exchange by EPEC is PKC mediated. Am J Physiol Gastrointest Liver Physiol 2006; 291:G959–G968.
55. Tse CM, Levine SA, Yun CH, Brant SR, Pouyssegur J, Montrose MH, Donowitz M. Functional characteristics of a cloned epithelial Na+/H+ exchanger (NHE3): resistance to amiloride and inhibition by protein kinase C. Proc Natl Acad Sci U S A 1993;90:9110–9114.
56. Vina-Vilaseca A, Bender-Sigel J, Sorkina T, Closs EI, Sorkin A. Protein kinase C-dependent ubiquitination and clathrin-mediated endocytosis of the cationic amino acid transporter CAT-1. J Biol Chem 2011; 286:8697–8706.
57. García-Tardón N, González-González IM, Martínez-Villarreal J, Fernández-Sánchez E, Giménez C, Zafra F. Protein kinase C (PKC)-promoted endocytosis of glutamate transporter GLT-1 requires ubiquitin ligase Nedd4-2-dependent ubiquitination but not phosphorylation. J Biol Chem 2012;287:19177–19187.
58. Xu D, Wang H, Zhang Q, You G. Nedd4-2 but not Nedd4-1 is critical for protein kinase C-regulated ubiquitination, expression, and transport activity of human organic anion transporter 1. Am J Physiol Renal Physiol 2016; 310:F821–F831.
59. Collazo R, Fan L, Hu MC, Zhao H, Wiederkehr MR, Moe OW. Acute regulation of Na+/H+ exchanger NHE3 by parathyroid hormone via NHE3 phosphorylation and dynamin-dependent endocytosis. J Biol Chem 2000; 275:31601–31608.
60. Liu T, Jose PA. Gastrin induces sodium-hydrogen exchanger 3 phosphorylation and mTOR activation via a phosphoinositide 3-kinase-/protein kinase C-dependent but AKT-independent pathway in renal proximal tubule cells derived from a normotensive male human. Endocrinology 2013;154:865–875.
61. Hu MC, Di Sole F, Zhang J, McLeroy P, Moe OW. Chronic regulation of the renal Na(+)/H(+) exchanger NHE3 by dopamine: translational and posttranslational mechanisms. Am J Physiol Renal Physiol 2013; 304:F1169–F1180.
62. Kocinsky HS, Dynia DW, Wang T, Aronson PS. NHE3 phosphorylation at serines 552 and 605 does not directly affect NHE3 activity. Am J Physiol Renal Physiol 2007; 293:F212–F218.
63. Chow CW, Khurana S, Woodside M, Grinstein S, Orlowski J. The epithelial Na(+)/H(+) exchanger, NHE3, is internalized through a clathrin-mediated pathway. J Biol Chem 1999;274:37551–37558.
64. Mayers JR, Wang L, Pramanik J, Johnson A, Sarkeshik A, Wang YJ, Saengsawang W, Yates JR, Audhya A. Regulation of ubiquitin-dependent cargo sorting by multiple endocytic adaptors at the plasma membrane. Proc Natl Acad Sci U S A 2013; 110:11857–11862.
65. Piper RC, Dikic I, Lukacs GL. Ubiquitin-dependent sorting in endocytosis. Cold Spring Harb Perspect Biol 2014; 6.
66. Sigismund S, Woelk T, Puri C, Maspero E, Tacchetti C, Transidico P, Di Fiore PP, Polo S. Clathrin-independent endocytosis of ubiquitinated cargos. Proc Natl Acad Sci U S A 2005;102:2760–2765.
67. Henry AG, Hislop JN, Grove J, Thorn K, Marsh M, von Zastrow M. Regulation of endocytic clathrin dynamics by cargo ubiquitination. Dev Cell 2012;23:519–532.
68. Wolfe BL, Marchese A, Trejo J. Ubiquitination differentially regulates clathrin-dependent internalization of protease-activated receptor-1. J Cell Biol 2007; 177:905–916.
69. Traub LM, Lukacs GL. Decoding ubiquitin sorting signals for clathrin-dependent endocytosis by CLASPs. J Cell Sci 2007;120:543–553.
70. Amin MR, Malakooti J, Sandoval R, Dudeja PK, Ramaswamy K. IFN-{gamma} and TNF-{alpha} regulate human NHE3 gene expression by modulating the Sp family transcription factors in human intestinal epithelial cell line C2BBe1. Am J Physiol 2006;291:C887–C896.
71. Pinto D, Robine S, Jaisser F, El Marjou FE, Louvard D. Regulatory sequences of the mouse villin gene that efficiently drive transgenic expression in immature and differentiated epithelial cells of small and large intestines. J Biol Chem 1999;274:6476–6482.
72. Babbin BA, Sasaki M, Gerner-Schmidt KW, Nusrat A, Klapproth JM. The bacterial virulence factor lymphostatin compromises intestinal epithelial barrier function by modulating rho GTPases. Am J Pathol 2009; 174:1347–1357.

73. Liang Z, Zhan W, Zhu A, Yoon Y, Lin S, Sasaki M, Klapproth J-MA, Yang H, Grossniklaus HE, Xu J, Rojas M, Voll RJ, Goodman MM, Arrendale RF, Liu J, Yun CC, Snyder JP, Liotta DC, Shim H. Development of a unique small molecule modulator of CXCR4. PLoS ONE 2012;7:e34038.
74. Kreis TE. Microinjected antibodies against the cytoplasmic domain of vesicular stomatis virus glycoprotein block its tranport to the cell surface. EMBO J 1986; 5:931–941.
75. He P, Lee SJ, Lin S, Seidler U, Lang F, Fejes-Toth G, Naray-Fejes-Toth A, Yun CC. Serum- and glucocorticoid-induced kinase 3 in recycling endosomes mediates acute activation of Na+/H+ exchanger NHE3 by glucocorticoids. Mol Biol Cell 2011;22:3812–3825.

Received September 27, 2021. Accepted November 15, 2021.

Correspondence
Address correspondence to: Chris Yun, PhD, Division of Digestive Diseases, Emory University School of Medicine, Atlanta, Georgia 30324. e-mail: ccyun@emory.edu; fax: (404) 727-5767.

Acknowledgments
The authors thank Drs Ghishan and Kiera for *Nhe3*$^{-/-}$ mice on FVB/N background.

CRediT Authorship Contributions

Kayte A. Jenkin, PhD (Conceptualization: Equal; Data curation: Lead; Formal analysis: Equal; Investigation: Equal; Methodology: Equal; Validation: Equal; Writing – original draft: Equal; Writing – review & editing: Supporting)

Yiran Han, MS (Conceptualization: Supporting; Data curation: Equal; Formal analysis: Equal; Investigation: Equal; Methodology: Equal; Validation: Equal; Writing – review & editing: Supporting)

Songbai Lin, MD (Data curation: Equal; Formal analysis: Equal; Investigation: Equal; Methodology: Equal; Validation: Supporting)

Peijian He, PhD (Data curation: Supporting; Formal analysis: Supporting; Methodology: Supporting; Writing – original draft: Equal)

Chris Yun, PhD (Conceptualization: Lead; Formal analysis: Equal; Funding acquisition: Lead; Investigation: Equal; Project administration: Lead; Supervision: Lead; Writing – original draft: Equal; Writing – review & editing: Lead)

Conflicts of interest
The authors disclose no conflicts.

Funding
Supported by grants from the National Institutes of Health (R01DK107719) and the Veterans Administration Merit Award (I01BX004459). Confocal microscopic analyses were supported in part by the Integrated Cellular Imaging Shared Resources of Winship Cancer Institute of Emory University and NIH/NCI under award P30CA138292.